

Elliptical galaxies at low surface brightness

Neill Reid,¹ Catherine Boisson² and A. E. Sansom³

¹California Institute of Technology, 105-24, Pasadena, CA 91126, USA

²D.A.E.C., Observatoire de Paris, Section de Meudon, UA 173, F-92195, Meudon, France

³Centre for Astrophysics, University of Central Lancashire, Preston PR1 2HE

Accepted 1994 March 8. Received 1994 February 8; in original form 1993 August 16

ABSTRACT

We present *BVI* CCD photometry of a sample of 11 elliptical galaxies chosen to cover a significant range in absolute luminosity. Our observations of the larger systems include exposures taken with the galaxy off-centre, allowing a better estimate of the true sky-background. We have used model-fitting to measure the structural parameters (ellipticity, position angle of the major axis, and the Fourier 4θ terms) of these systems, as well as determining the ($B - V$) and ($V - I$) colours as a function of radius. In contradiction to some previous observations, we find that none of the galaxies has significant, large-scale radial colour gradients. Three galaxies have shells or arcs – structure not previously detected in either NGC 3091 or NGC 4936.

Key words: galaxies: elliptical and lenticular, cD – galaxies: fundamental parameters – galaxies: photometry.

1 INTRODUCTION

At first sight, elliptical galaxies present the appearance of uncomplicated systems, with a simplicity of structure, absence of current activity and uniformity of character amongst galaxies spanning an absolute magnitude range of more than seven magnitudes. Detailed observations over the last two decades, however, have shown that this apparent simplicity is deceptive. First, there is a considerable range of kinematic properties. In the classical picture, the form – particularly the flattening – of elliptical galaxies stemmed from the overall rotation, but Bertola & Cappacioli (1975) provided the first evidence that ordered rotation is of significantly less importance in many ellipticals than it is in spirals. These observations, coupled with the availability of higher efficiency detectors, prompted a number of studies, with the main results being summarized by Davies et al. (1983). While lower luminosity ellipticals ($M_v \lesssim -20$) generally have properties consistent with Binney's (1978) models of rotationally supported oblate spheroids, the more luminous systems show a substantial range in properties, with most having little or no observed rotation. This implies that the ellipticity amongst the latter systems stems (at least in part) from anisotropic velocity dispersions, and raises the possibility of different formation scenarios for morphologically similar systems.

In a similar vein, recent morphological studies have also suggested that there may be more than one evolutionary path towards an elliptical-like system. It has long been known that the surface-brightness profiles of most ellipticals are well-

represented by an $r^{0.25}$ ‘law’ (de Vaucouleurs 1948, 1953), and Binney (1982) has shown that a projected isothermal distribution can mimic this profile. However, more detailed two-dimensional photometric studies – particularly in recent years, with the application of CCDs to the subject (Kent 1984; Lauer 1985; Djorgovski 1985; Jedrzejewski 1987, hereafter J87; Carter 1987; Bender, Döbereiner & Möllenhoff 1988; Vigroux et al. 1988; Bender et al. 1989; Franx, Illingworth & Heckman 1989, hereafter FIH; Peletier et al. 1990, hereafter PDIDC; Mackie, Visvanathan & Carter 1990; Jorgenson, Franx & Kjaergaard 1992, hereafter JFK) – have shown that many galaxies have significant and (in some cases) systematic deviations from a purely elliptical form. The latter fall within two broad groupings – those having pointed isophotes, generally interpreted as indicative of the presence of weak discs, and those with ‘boxy’ isophotes. Kinematically, most of the pointed-isophote systems are consistent with oblate systems with isotropic dispersion. In terms of the relative frequencies of the different types, Bender et al. (1989) classified approximately one-third of their sample as ‘pointed’ or ‘discy’, and a similar number as ‘boxy’. The remaining galaxies they classified as ‘irregular’, and, prompted mainly by the similarity of the radio properties, grouped these galaxies with the boxy systems, distinct from the radio-weak, S0-like ‘discy’ objects.

While most quantitative studies of the detailed photometric structure are (still) limited to relatively high surface brightnesses, some ellipticals also show structure in the outer regions – notably the shells around otherwise normal elliptical galaxies, first identified by Malin & Carter (1980).

Subsequent surveys, based on both photographic material (Malin & Carter 1983) and CCD data (Schweizer & Seitzer 1992), have revealed similar ripple-like features around many early-type systems, as well as more complex wisps and tails. These are generally interpreted as the signature of merger events, possibly of low-mass disc systems (Quinn 1984; Dupraz & Combes 1987). On a larger scale, the earliest simulations (Toomre & Toomre 1972) showed that merging two disc systems could produce an elliptical-like remnant, and observations of current mergers, such as NGC 7252 (Schweizer 1982) and Arp 220 (Wright et al. 1990), show that the underlying old population has an $r^{0.25}$ distribution. Given the prevalence of fine structure, Schweizer & Seitzer argue that nearly half of the galaxies in their sample, including both ellipticals and S0s, have undergone a merger within the last 7 Gyr. This raises the possibility that *all* early-type systems, including the ‘discy’, bulge-dominated S0s, may have undergone some merging during their evolution.

Besides pure morphological studies, one of the methods that has been applied to probing the evolutionary history of elliptical galaxies is searching for metallicity variations in these systems. Purely dissipational formation is expected to create abundance gradients, with the central regions of the system becoming more metal-rich as they are fuelled by infalling processed gas. Most scenarios predict that any such gradients will be weakened by subsequent merging, although Kormendy & Sanders (1992), based on a survey of ultraluminous *IRAS* galaxies, have suggested that the additional dissipation and gaseous infall may *strengthen* abundance gradients. Direct spectroscopic observations have shown that significant abundance gradients are indeed present within some (normal) ellipticals, although in other systems there is little or no change in the mean metallicity with radius (Gorgas, Efstathiou & Aragon-Salamanca 1990, hereafter GES; Boroson & Thompson 1991; Delisle & Hardy 1992; Davidge 1992; Davies, Sadler & Peletier 1993, hereafter DSP; Carollo, Danziger & Buson 1993). Moreover, in many systems that have abundance variations, the gradients are weak or non-existent outside the immediate vicinity of the nucleus.

Spectroscopy is clearly the most direct means of measuring metallicity variations in elliptical galaxies. With a bandpass of only 5–10 Å, however, signal-to-noise ratio considerations generally limit such investigations to within the effective radius, R_e . Direct imaging allows one to expand the bandpass and extend coverage to lower surface-brightness levels (and to two dimensions), but at the expense of complicating the interpretation of the results. Higher metal abundance leads to higher line-blanketing and redder optical colours in the giant branch stars, which dominate the light in older stellar populations; near solar abundance, a change of $\Delta[\text{Fe}/\text{H}]$ of 0.5 dex leads to $\Delta(B-R)$ of 0.1 mag (Peletier 1989), or ~ 0.05 mag in $(B-V)$ and ~ 0.1 mag in $(V-I)$. However, either dust absorption or age differences in the stellar populations [such as the presence of intermediate age asymptotic giant branch (AGB) stars] can provoke similar photometric variations. Hence, while broad-band observations open up to investigation the outer regions of ellipticals, any conclusions concerning abundance gradients must be tempered by the inherent ambiguities of interpretation.

Despite these interpretative problems, broad-band observations are the only means of probing below $\Sigma_v \sim 22$ mag arcsec $^{-2}$, and there have been many searches for colour gradients in early-type systems. Most studies are based on *UBR* data, and generally agree in finding relatively strong gradients in $(U-R)$, and milder gradients [~ 0.1 mag $(\log r)^{-1}$] in $(B-R)$. In most cases, the galaxy appears to become bluer (more metal-poor) with increasing radius (the main exceptions are the cooling-flow galaxies surveyed by McNamara & O’Connell 1992). These gradients, however, are barely significant when one takes into account possible systematic errors in the adopted sky brightness (FIH, JFK) – a problem that reflects the small areal coverage (typically 2.5×4.0 arcmin 2) of the observations in all previous surveys. Moreover, there are significant discrepancies between different sets of observations, concerning both individual galaxies and more global characteristics. Vader et al. (1988), for example, find that the colour gradient correlates with both the luminosity (their low-luminosity ellipticals appear to become redder at large radii) and rotational properties. Neither correlation has been confirmed by FIH, PDIDC or JFK.

Given these discrepancies, we obtained deep, multi-colour observations of a small sample of elliptical galaxies with the aim of addressing both the question of the radial extent of any colour gradients and the frequency of fine structure. Our sample, although small, is chosen to span a significant range of absolute luminosity, and, in order to reduce the uncertainties in the determination of the sky-background, we have taken overlapping offset frames for the larger galaxies. In addition, we have undertaken observations in the *BVI* passbands; with the longer baseline in wavelength, colour gradients in $(B-I)$ should have nearly twice the amplitude of those in $(B-R)$. [Gradients in $(V-I)$ should be at least comparable to those in $(B-R)$.] In the following section, we outline our observations and data reduction; in Section 3, we present our results for the individual systems; in Section 4, we discuss the question of colour gradients in ellipticals and the overall structure of the galaxies in our sample; finally, in Section 5, we summarize our conclusions.

2 PHOTOMETRY

We have already presented an extensive analysis of one of the galaxies in our sample, NGC 6776 (Sansom, Reid & Boisson 1988, hereafter SRB), and the observations and many of the data reduction techniques that we have employed are described in that paper. The following sections summarize those procedures.

2.1 Observations

Our CCD data were obtained using the Danish 1.5-m telescope at ESO, La Silla, between 1985 April 24/25 and 1985 April 29/30. The detector was a thinned, back-illuminated 320×512 RCA device with $30 \mu\text{m}$ (0.47 arcsec) pixels and we used *B*, *V* (Johnson) and (Gunn) *i*-band filters. As one of the main aims of our observations was the study of the outer isophotes of the galaxies in our sample, we have obtained overlapping offset frames of the larger systems, and in most cases this provides ample coverage for sky

determination. Table 1 lists the galaxies in our sample and shows the total integration time accumulated in each passband. Some of our observations were obtained while the moon was up, and we have listed the sky brightness for each of the galaxy-centred exposures. Conditions were photometric on all except one of the observing nights, and NGC 5831 is the only galaxy that was not observed under photometric conditions on another night. We have been able to use previously published photometry to establish the zero-points for that galaxy, as discussed further in Section 2.3. The seeing conditions during our observing run were generally very good to excellent, with stellar images having a FWHM of from 0.6 to 1.3 arcsec. The central regions of several galaxies (NGC 2865, 3091, 3557, 4936 and 5845) are saturated on our longer exposures, and, in most cases, we have not attempted to probe within 4 arcsec in these systems.

2.2 Data reduction

Each CCD frame was bias-subtracted and flat-fielded using standard techniques. As described in SRB, we have allowed for a small, non-linear dark current of 3×10^{-3} count pixel $^{-1}$ s $^{-1}$ in the bias subtraction. The lower left (SW) corner of the RCA chip is 'hot', and, rather than attempt to correct for the excess counts, we have excised a 50×30 pixel area where this interferes with the galactic photometry. We took both dome flats and twilight-sky exposures, but (like JFK) found that the former gave unacceptable large-scale residuals and we therefore used only the latter frames to flat-field our data.

The individual frames were aligned and then merged using Starlink software. As we described in SRB, in several cases separate exposures of the same field (or of overlapping fields) were made on different nights under different conditions of transparency and zenith distance (multiplicative changes in intensity level) or of moonlight and sky brightness (additive changes in the background level). In those cases, rather than attempting to calibrate separately the intensity change in the sky and object, we have used all the pixels in the overlap region to define an empirical transform-

mation as a function of the observed intensity, matching the data from the offset frame to the scale of the central frame. This leads to discontinuities in intensity of at most 0.35 per cent of the sky-background (typical values are 0.2–0.25 per cent) at the boundaries of the overlap region. These uncertainties are comparable with the limitations that are set by the accuracy of our flat-fielding – measuring the median sky brightness in 20–30 regions (uncontaminated by galaxies) on several frames gives a typical rms scatter of ± 0.5 per cent. Finally, we have used two-dimensional polynomial interpolation to patch over the brighter galactic stars on the main body of the galaxies. The final images are presented in Fig. 1 (opposite p. 716).

2.3 Aperture photometry

In addition to our deep integrations, we obtained 1-min exposures of each galaxy, and we have used aperture photometry to measure the curve of growth for each system to a radius of 28 arcsec. Our photometry is calibrated through observations of standard stars in M67 (Eggen & Sandage 1964; Schild 1983) and in the Galactic structure fields set up by Stobie et al. (1987). (Although we used a Gunn *i* filter, our magnitudes are tied to the Cousins zero-point.) Defining

$$b/v/i = -2.5 \log(N_c),$$

where N_c is the count-rate in adu s $^{-1}$, then

$$B = 21.53 \pm 0.04 + b + k_b \sec z,$$

$$V = 21.59 \pm 0.03 + v + k_v \sec z,$$

$$I_c = 20.16 \pm 0.04 + i + k_i \sec z,$$

where we have adopted the standard ESO values of 0.2, 0.1 and 0.05 for the respective extinction coefficients. (All of the galaxies were observed at airmasses of less than 1.2 except for NGC 4387, where the airmass reached 1.5.) The dark-of-moon sky brightnesses that we derive are $B = 22.82$, $V = 21.69$ and $I = 19.71$.

Our observations include standard stars covering only a limited range in colour, $0.5 < (V-I) < 0.8$, which is insufficient to derive accurate colour terms. JFK derive such terms for the same system (albeit six years after our observations) and find a slope of ~ 0.04 per mag in $\delta(B-V)$. Since the galaxies are at most 0.2 mag redder than the reddest standard, any systematic offsets are negligible compared with the random uncertainties. Table 2 lists the results of our photometry, where we present both the integrated colours within each aperture and the differential colours derived for the corresponding annulus. None of the galaxies shows evidence of significant colour terms in $(V-I)$, and although a few systems (such as NGC 4936 and 6851) have bluer $(B-V)$ colours at larger radii, the effect is only marginally significant.

As an external comparison, all of the galaxies in our sample (except NGC 3091A, the companion to NGC 3091) were observed in the Burstein et al. (1987) survey. We have adopted their estimates for the line-of-sight reddening towards each galaxy and for the effective circular diameters, A_e , of each system. We also follow their prescription in applying K corrections (from RC2) and correcting for the $(1+z)^4$ cosmological effect on surface brightness. Based on these data, together with the standard curve of growth

Table 1. The galaxies in our sample. Column 1 lists the NGC number, column 2 the effective diameter in arcsec, column 3 the absorption (in mag) along the line of sight in the blue passband, columns 4–6 give the total exposure times (in min) for the frames with the galaxy centred in the field, and columns 7–9 list the exposure times in the offset fields. (The three dwarf systems, NGC 4387, 5831 and 5845 did not require the latter observations.) Columns 10–12 show the sky brightness (in mag) for each of the exposures with the galaxy centred on the chip. A_e and A_B are taken from Burstein et al. (1987).

NGC	A_e	A_B	Galaxy			Exposure times			Sky brightness		
			B	V	I	centre	offset	B	V	I	B
2865	23	0.27	30	30	30	30	30	20.7	20.2	19.1	
3091	61	0.14	30	30	30	30	30	22.8	21.7	19.7	
3258	55	0.26	30	30	30	30	30	22.4	21.6	19.4	
3268	72	0.26	30	30	30	30	30	20.4	20.0	18.8	
3557	76	0.33	30	30	30	30	30	21.8	21.1	19.2	
4387	31	0.13	20	30					20.5	19.0	
4936	112	0.34	30	30	30	30	30	22.7	21.5	19.9	
5831	54	0.14	30	30	30				22.7	21.3	19.6
5845	8	0.14	30	30	30				22.8	21.3	19.5
6851	29	0.07	20	30	30			21.3	21.5	19.5	
6909	62	0.07	30	30	20	30	30	22.7	21.4	19.0	

Table 2. Aperture photometry of the galaxies in our sample. Column 1 lists the radius, in arcsec, columns 2–6 the cumulative magnitudes and colours, and columns 7 and 8 the differential colours of the individual annuli.

		NGC 2865							
r "		B	V	I	B-V	V-I	B-V	V-I	
				cum.		diff.			
4.7	14.24	13.29	12.09	0.94	1.20	0.94	1.20	1.15	1.22
9.4	13.58	12.64	11.46	0.94	1.18	0.94	1.16	1.12	1.30
14.1	13.33	12.38	11.16	0.95	1.21	0.97	1.31	1.11	1.32
18.8	13.16	12.20	10.97	0.96	1.23	1.04	1.33	1.12	1.36
23.5	13.06	12.09	10.84	0.98	1.25	1.11	1.41	1.12	1.36
28.2	13.00	12.01	10.74	0.99	1.27	1.23	1.48	1.14	1.38
NGC 3091									
4.7	14.62	13.51	12.17	1.12	1.34	1.12	1.34	1.13	1.31
9.4	13.99	12.90	11.56	1.09	1.34	1.06	1.34	1.09	1.30
14.1	13.68	12.58	11.24	1.10	1.34	1.14	1.34	1.09	1.30
18.8	13.49	12.39	11.05	1.10	1.34	1.10	1.36	1.07	1.31
23.5	13.35	12.25	10.90	1.10	1.35	1.10	1.37	1.07	1.32
28.2	13.26	12.15	10.79	1.11	1.35	1.16	1.42	1.07	1.32
NGC 3091A									
4.7	15.45	14.31	12.98	1.14	1.33	1.14	1.33	1.00	1.25
9.4	15.17	14.04	12.69	1.13	1.35	1.12	1.43	1.01	1.25
14.1	15.04	13.92	12.52	1.11	1.40	0.96	1.74	1.01	1.26
18.8	14.95	13.84	12.40	1.11	1.44	1.01	1.91	1.01	1.29
NGC 3258									
4.7	14.87	13.75	12.32	1.12	1.43	1.12	1.43	1.02	1.28
9.4	14.20	13.08	11.68	1.12	1.40	1.12	1.36	1.02	1.28
14.1	13.89	12.76	11.35	1.13	1.41	1.17	1.43	1.02	1.28
18.8	13.70	12.57	11.15	1.13	1.42	1.15	1.49	1.02	1.30
23.5	13.58	12.44	11.00	1.14	1.43	1.21	1.53	1.02	1.30
28.2	13.50	12.35	10.90	1.15	1.45	1.24	1.59	1.02	1.31
NGC 3268									
4.7	15.07	13.88	12.41	1.19	1.47	1.19	1.47	1.01	1.25
9.4	14.32	13.21	11.73	1.11	1.47	1.02	1.47	1.01	1.25
14.1	14.00	12.89	11.41	1.11	1.48	1.11	1.49	1.01	1.26
18.8	13.81	12.69	11.20	1.12	1.49	1.19	1.55	1.02	1.30
23.5	13.67	12.54	11.03	1.14	1.51	1.21	1.63	1.02	1.30
28.2	13.56	12.41	10.89	1.15	1.52	1.31	1.55	1.02	1.29
NGC 3557									
4.7	14.00	12.94	11.57	1.15	1.37	1.15	1.37	1.02	1.28
9.4	13.38	12.25	10.86	1.14	1.38	1.12	1.40	1.02	1.28
14.1	13.06	11.93	10.54	1.13	1.39	1.12	1.41	1.02	1.28
18.8	12.87	11.73	10.33	1.14	1.40	1.18	1.43	1.02	1.28
23.5	12.72	11.58	10.18	1.13	1.41	1.11	1.47	1.02	1.28
28.2	12.60	11.47	10.05	1.14	1.41	1.16	1.48	1.02	1.28
NGC 4387									
4.7	13.87	12.59		1.28		1.28		1.02	1.28
9.4	13.17	11.86		1.30		1.33		1.02	1.28
14.1	12.86	11.53		1.32		1.38		1.02	1.28
18.8	12.69	11.33		1.36		1.53		1.02	1.28
23.5	12.58	11.19		1.39		1.70		1.02	1.28
28.2	12.51	11.07		1.44		1.98		1.02	1.28
NGC 4936									
4.7	14.91	13.69	12.19	1.23	1.50	1.23	1.50	1.02	1.28
9.4	14.05	12.88	11.43	1.17	1.45	1.12	1.41	1.02	1.28
14.1	13.57	12.42	10.98	1.15	1.44	1.13	1.41	1.02	1.28
18.8	13.31	12.16	10.74	1.15	1.42	1.14	1.35	1.02	1.28
23.5	13.14	11.99	10.58	1.15	1.42	1.14	1.40	1.02	1.28
28.2	13.03	11.88	10.46	1.15	1.42	1.18	1.42	1.02	1.28
NGC 5831*									
4.7	15.29	14.19	13.09	1.10	1.10	1.10	1.10	1.02	1.28
9.4	14.63	13.54	12.39	1.09	1.14	1.07	1.19	1.02	1.28
14.1	14.31	13.21	12.04	1.10	1.17	1.12	1.24	1.02	1.28
18.8	14.12	13.02	11.83	1.10	1.19	1.12	1.27	1.02	1.28
23.5	13.99	12.88	11.68	1.11	1.20	1.17	1.33	1.02	1.28
28.2	13.90	12.78	11.56	1.11	1.23	1.16	1.47	1.02	1.28

Table 2 – continued

r "		NGC 5845		I	B-V	V-I	B-V	V-I
		r "	B	V	cum.	diff.		
4.7		4.7	14.29	13.14	11.91	1.15	1.22	1.15
9.4		9.4	13.94	12.82	11.52	1.12	1.30	1.05
14.1		14.1	13.82	12.71	11.39	1.11	1.32	0.97
18.8		18.8	13.77	12.66	11.32	1.11	1.33	1.13
23.5		23.5	13.75	12.62	11.27	1.12	1.36	1.03
28.2		28.2	13.74	12.61	11.22	1.14	1.38	2.95
NGC 6851								
4.7		4.7	14.64	13.51	12.20	1.13	1.31	1.13
9.4		9.4	14.02	12.93	11.63	1.09	1.30	1.03
14.1		14.1	13.74	12.65	11.35	1.09	1.30	1.09
18.8		18.8	13.55	12.48	11.18	1.07	1.30	0.98
23.5		23.5	13.43	12.37	11.06	1.07	1.31	1.01
28.2		28.2	13.36	12.29	10.98	1.07	1.32	1.13
NGC 6909								
4.7		4.7	15.04	14.04	12.79	1.00	1.25	1.00
9.4		9.4	14.36	13.36	12.11	1.00	1.25	1.01
14.1		14.1	14.01	13.00	11.74	1.01	1.26	1.03
18.8		18.8	13.81	12.79	11.51	1.02	1.28	1.03
23.5		23.5	13.68	12.66	11.36	1.02	1.30	1.10
28.2		28.2	13.59	12.54	11.24	1.05	1.30	1.31

*The NGC 5831 observations were affected by cloud and require zero-point corrections of -0.65 mag (see text).

that they derive, we have computed the total magnitudes listed in Table 3. By comparing our results with the B , V data listed by Burstein et al., we find mean differences of $\Delta B = 0.15 \pm 0.06$, 9 systems, and $\Delta V = 0.06 \pm 0.04$, 10 systems, in the sense that our magnitude estimates are fainter.¹ Systematic offsets of this size are unimportant for the present purposes, where we are concerned primarily with differential photometry within each system. The absolute visual magnitudes, which are calculated only for reference, have been computed from the Hubble-flow velocities listed in Faber et al. (1989), adopting (for convenience) a Hubble parameter of $100 \text{ km s}^{-1} \text{ Mpc}^{-1}$.

2.4 Surface photometry

We have used two methods in our analysis of the CCD images. First, we have applied the PLEINPOT software (Stavelli, Prugniel & Zeilinger 1991) to derive azimuthally averaged surface-brightness profiles, as well as the run of ellipticity, major-axis orientation and Fourier coefficients (particularly the 4θ terms) with radius. These routines also allow construction of a model galaxy, which, when subtracted from the observed image, can be used to reveal the presence of shells, jets or other irregular structures. In

¹NGC 5831 was observed through thin cloud and we have established the zero-points for the aperture photometry using the surface photometry by J87 and PDIDC. Note that JFK give the effective radius as 19.8 arcsec, rather than 27 arcsec (Burstein et al. 1987); adoption of the smaller radius leads to a decrease in the total magnitude of ~ 0.25 mag.

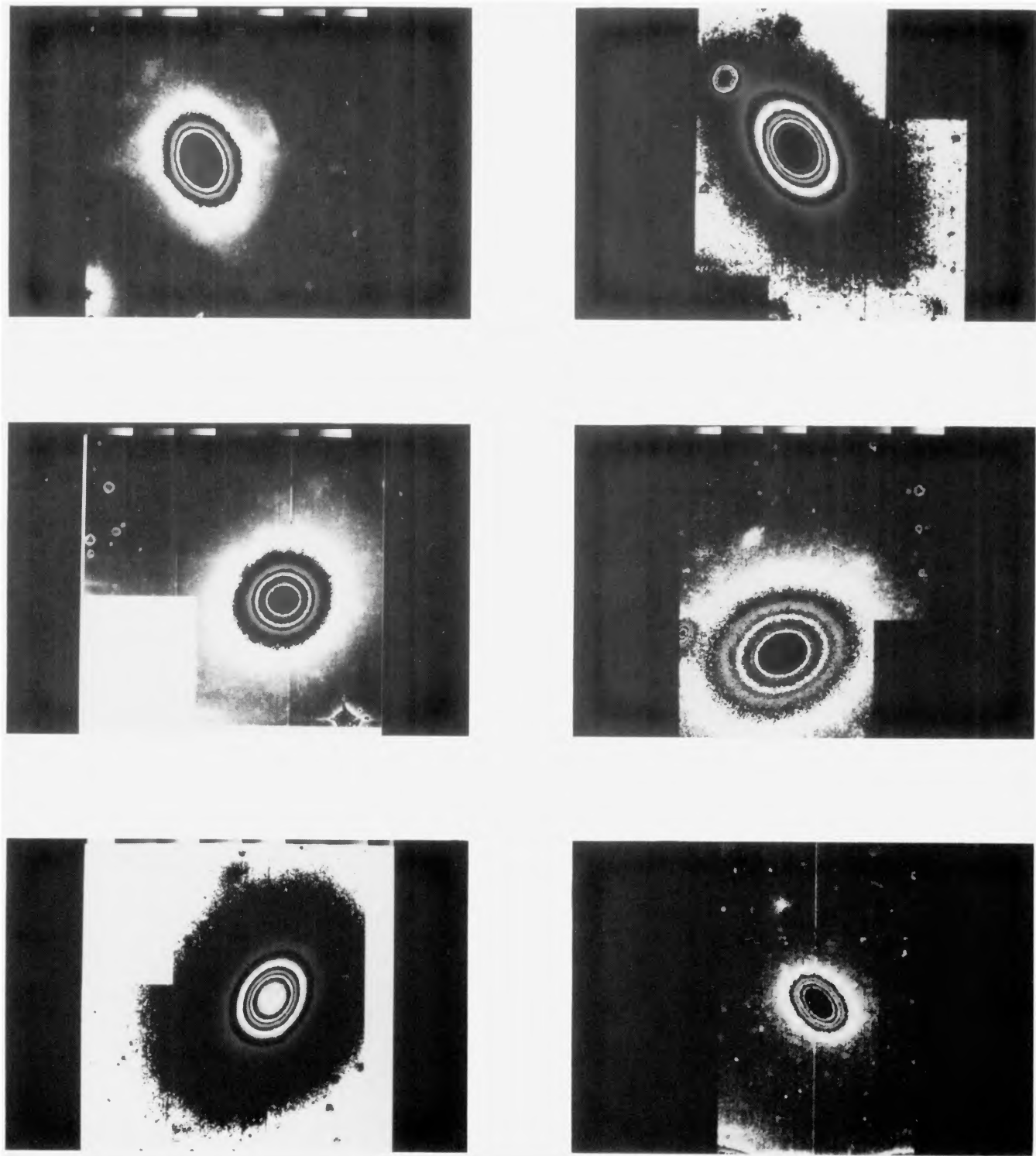


Figure 1. (a) Composite CCD images of six of the 11 galaxies in our sample: top left: NGC 2865; top right: NGC 3091; middle left: NGC 3258; middle right: NGC 3268; bottom left: NGC 3557; bottom right: NGC 4387. All are plotted with north at the top and east on the right. Bright stars within ~ 100 arcsec of the centre of each galaxy have been patched over, although low-level residuals are still evident in some cases (for example, the apparent string of low-surface-brightness features lying to the north of NGC 3258).

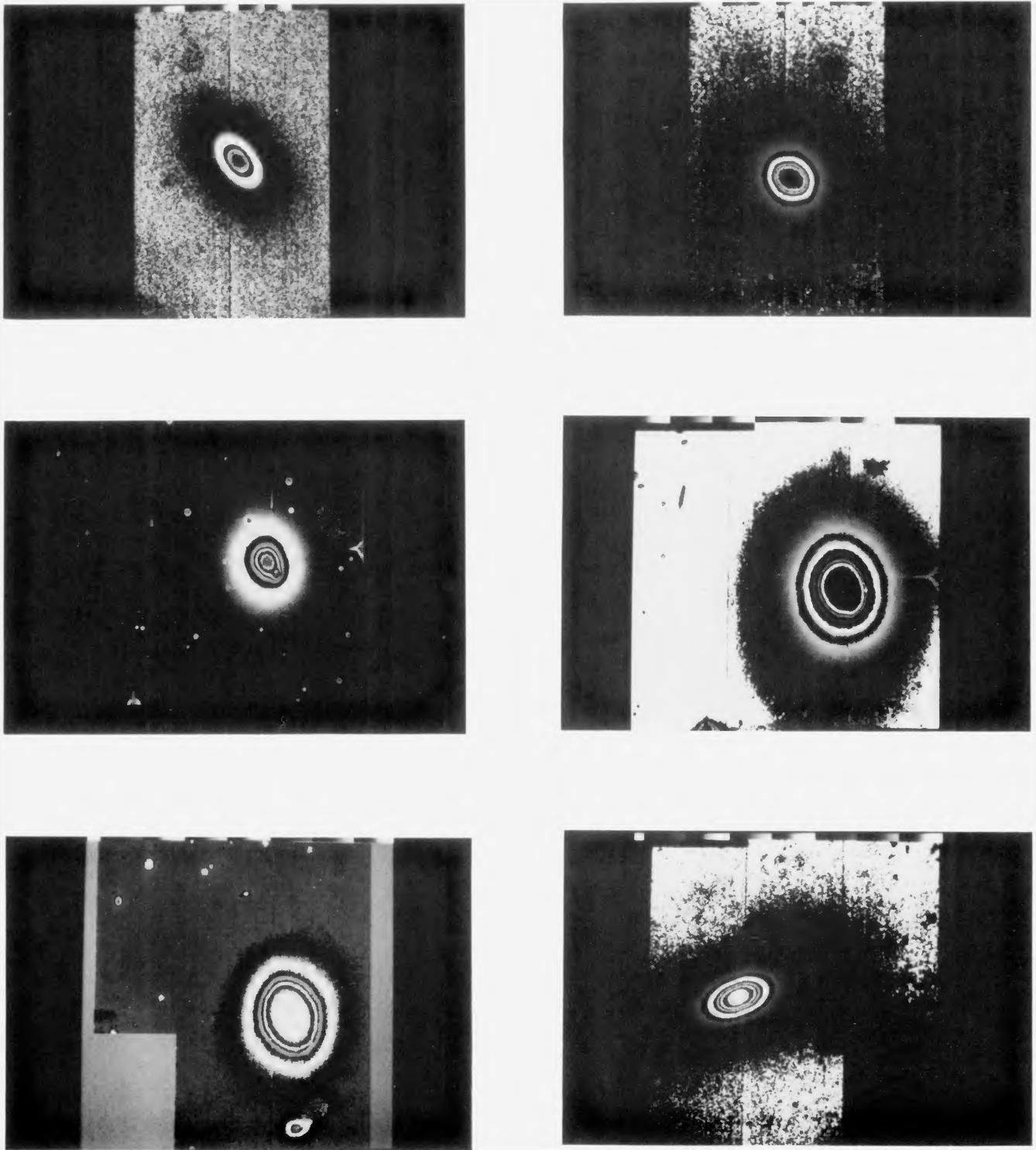


Figure 1. (b) CCD images of the remaining five galaxies in our sample: top left: NGC 5845; top right: NGC 5831; middle: NGC 4936, with the grey-scale of the left-hand image set to show the double nucleus; bottom left: NGC 6851; bottom right: NGC 6909.

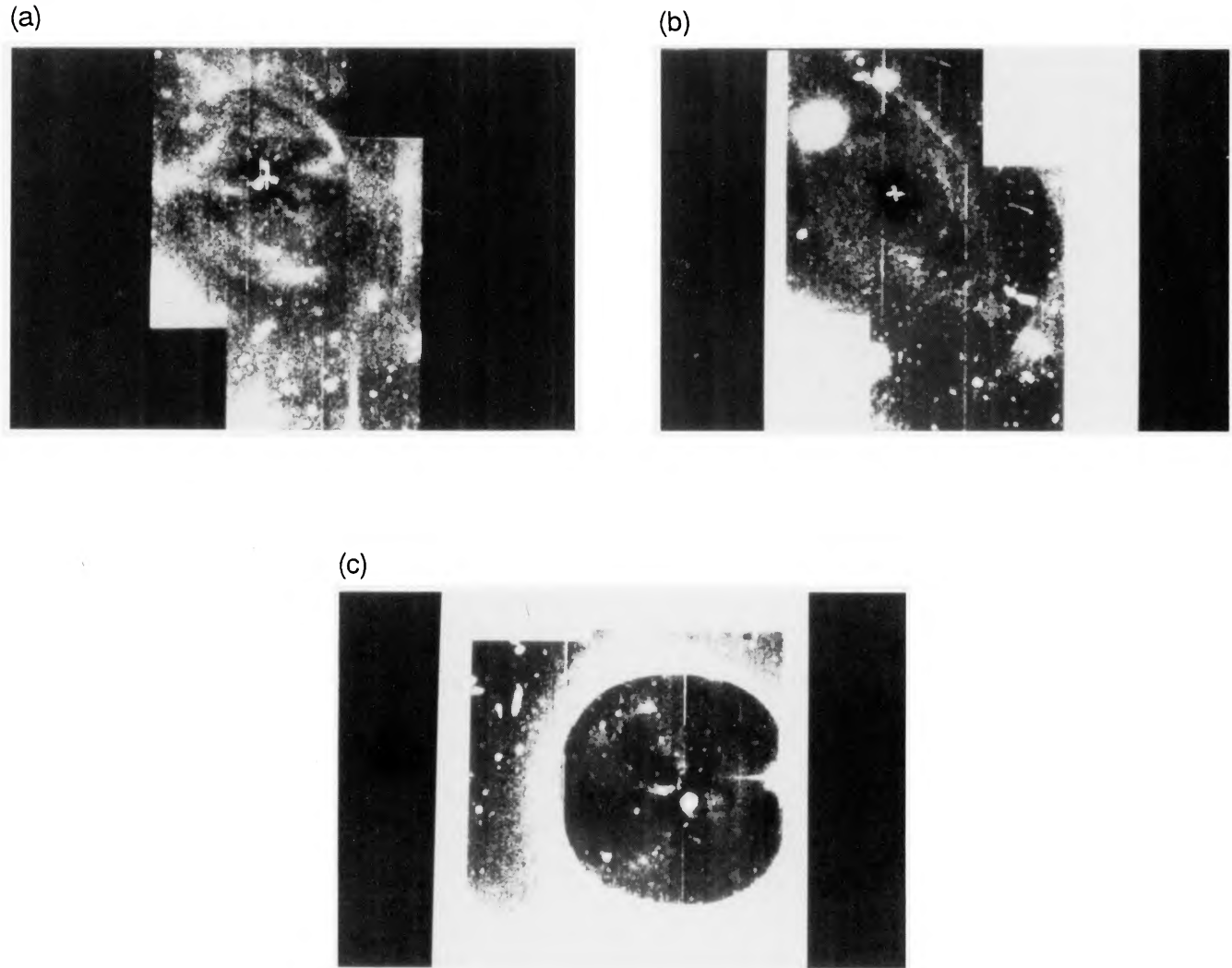


Figure 14. These figures show the residuals left after subtracting PLEINPOT models of three galaxies. (a) NGC 2865; (b) NGC 3091; (c) NGC 4936.

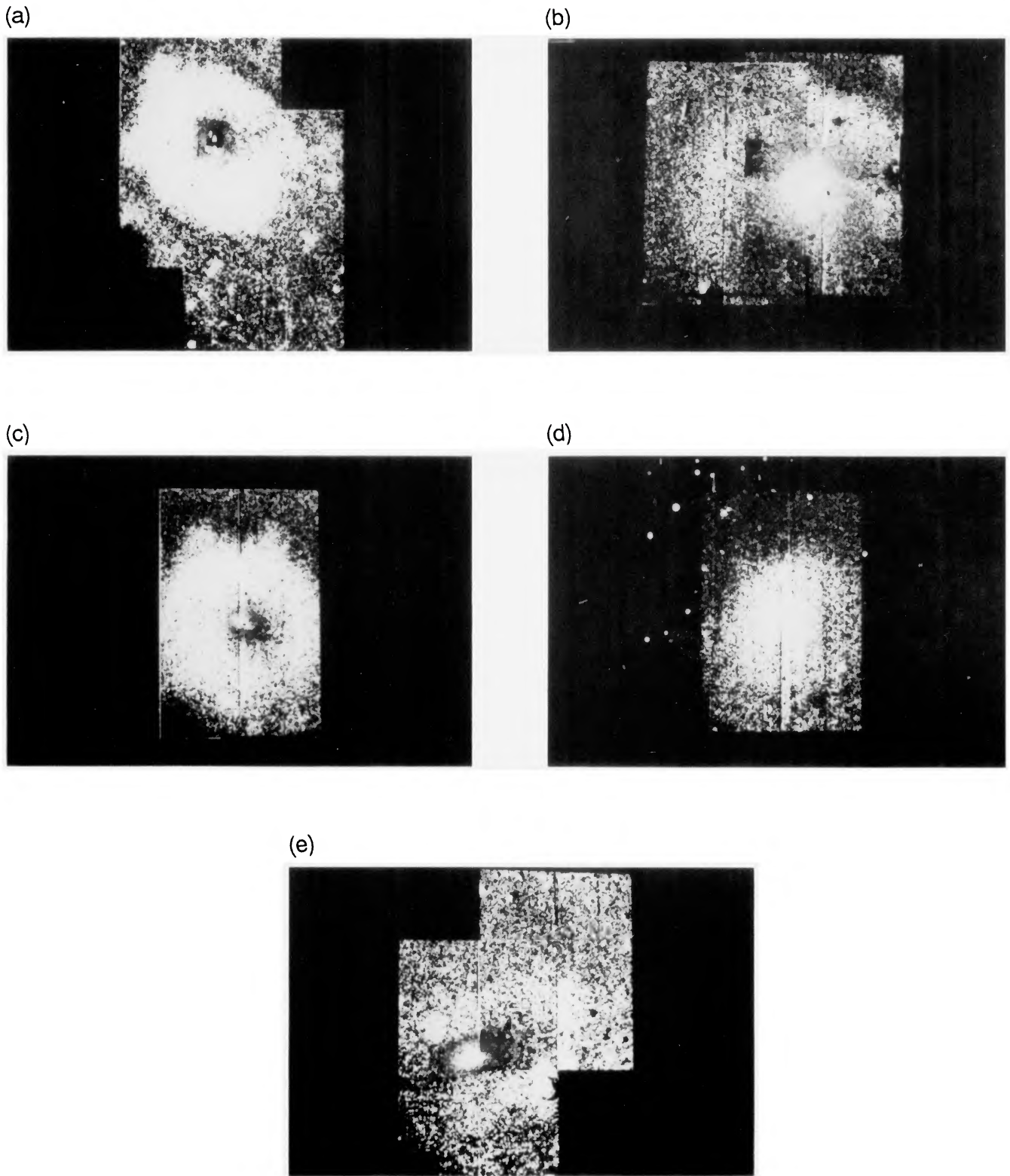


Figure 15. ($B - I$) colour maps for galaxies from our sample: (a) NGC 2865 – our data suggest a patch of extinction lying ~ 7 arcsec to the SE of the nucleus; (b) NGC 4936 – the nuclear regions are significantly redder than the rest of the galaxy; (c) NGC 5831 – our data provide some support for the presence of a central disc or dust lane; (d) NGC 6851 – the red nucleus is clearly evident, together with a dust lane (?) running north-south. Note that we have no offset frame in B for this system; (e) NGC 6909 – like NGC 6851, this system has a very red nucleus.

Table 3. Total magnitudes for the galaxies in our sample. These have been computed from the $r=28.2$ -arcsec aperture photometry listed in Table 2 by using the curve of growth given in Burstein et al. (1987). The absolute magnitudes are based on the expansion velocities given in Faber et al. (1989), with $H_0 = 100 \text{ km s}^{-1} \text{ Mpc}^{-1}$. ΔB and ΔV are the magnitude differences with respect to Burstein et al. (1987).

NGC	V_t	M_v	$(B - V)_t$	$(V - I)_t$	ΔB	ΔV
2865	11.49	-19.6	0.89	1.15	0.09	0.03
3091	11.25	-21.8	1.04	1.27	0.20	0.13
3258	11.36	-21.3	1.06	1.32	0.13	0.07
3268	11.29	-21.2	1.06	1.39	0.12	0.04
3557	10.18	-21.7	1.03	1.27	0.08	0.02
4387	12.00	-18.6		1.36		0.05
4936	10.33	-21.7	1.03	1.27	0.16	0.09
5831*	11.29	-20.6	1.06	1.15		
5845	12.37	-19.5	1.08	1.31	0.10	0.00
6851	11.76	-20.0	1.01	1.24	0.21	0.10
6909	11.65	-20.2	1.01	1.25	0.25	0.10

*NGC 5831 data have been adjusted by -0.65 mag to match the J87 surface photometry.

addition to the azimuthally averaged photometry, we have derived surface-brightness profiles for specific position angles (typically the data encompass $\pm 15^\circ$ in θ). The sky-background level for these data has been defined as the median intensity in regions least contaminated by galactic light. Because systematic variations of up to 0.3 per cent in the background can be introduced by the image mosaicking and flat-fielding, however, we have calculated Σ_V profiles for sky values 0.5 per cent both above and below the best-fitting estimates. These better represent the actual uncertainties in photometry at such low light levels.

Most of the galaxies included in our sample have been observed previously, mainly in the *UBR* passbands. We have compared our observations against data from three of the more extensive surveys: J87 (nine galaxies in common), PDIDC (three galaxies in common: NGC 4387, 5831 and 5845) and JFK (three galaxies in common: NGC 2865, 3091 and 3268). Each of these three groups has conducted a thorough comparison between their observations and others in the literature; indeed, Jedrzejewski's (J87) photometric zero-points are explicitly defined with reference to previously published aperture photometry. In addition, Sparks et al. (1991) have derived averaged profiles for NGC 6851 and 6909, and we have compared these data against our own observations.

We have plotted the relevant surface photometry in Figs 2(a)–(j), plotting data from J87 as solid squares, data from PDIDC as open triangles and data from JFK as open circles. All three publications provide *B*-band surface brightnesses for the major-axis profile, and the lines define the major-axis profiles derived from our own observations. To avoid confusion arising from seeing variations and/or saturation, we have truncated our data at an inner radius of 2 arcsec ($r^{0.25} \sim 1.2$). We have no *B*-band observations of NGC 4387, but have plotted the *V*-band profile scaled by $(B - V) = 0.92$ (Burstein et al. 1987).

All of the observations match well at high surface brightnesses ($\Sigma_B < 23$). While our data are in good agreement with the JFK and Sparks et al. results at fainter levels, there are significant discrepancies with respect to some of

the J87 and PDIDC profiles, with our observations falling progressively further below the latter's photometry with increasing radius. This offset could be produced either by our overestimating, or by J87's (PDIDC's) underestimating, the true sky-background. JFK found similar differences between their observations and J87's for a number of other galaxies, while PDIDC found good agreement between their *B*-band data and J87's. (In the latter case, however, discrepancies were present in the comparison of the *R*-band observations.) Jedrzejewski's CCD frames² covered only $2.5 \times 4.0 \text{ arcmin}^2$. Given the larger areal coverage of our observations – and the excellent agreement with JFK's data – we believe that the lower surface brightnesses derived from our observations are likely to be the more accurate.

3 THE INDIVIDUAL SYSTEMS

In this section we consider the characteristics of each of the 11 galaxies in our sample (Table 4). We have calculated the major- and minor-axis photometric profiles of each galaxy using our own routines, and the results are displayed for each system in Figs 3–13. In addition, we have plotted the eccentricity, position angle of the major axis, the $\cos(4\theta)(a_4)$, and $\sin(4\theta)(b_4)$ Fourier coefficients as functions of the averaged radius, $r = \sqrt{ab}$, where a and b are the lengths of the major and minor axes, respectively. The latter data are also listed in Tables 5–15. The position angles are measured from north through east. In our calculation of photometric profiles on the principal axes, we have computed the effect of changing the sky-background by 0.5 per cent, and the results are shown for each galaxy. We have also derived the major-axis colour profiles, and, again, have computed the effect of a 0.5 per cent miscalculation in the sky levels. The 1σ lines plotted show the *maximum* effect on the colours (i.e. errors in opposite senses in the two frames).

Table 4 provides some general information on the environment and the overall structure (based on our analysis) of the galaxies in our sample. In addition, we list the colour (and abundance) gradients derived from previous observations, with a negative gradient implying bluer colours at larger radii – note that J87 finds several galaxies to have positive gradients. We do not find significant colour gradients for any of the galaxies in our sample. Particular details of each system are discussed in the following paragraphs.

NGC 2865. This is one of the classical shell galaxies (Malin & Carter 1983). After subtracting our model galaxy from the data (Fig. 14a, opposite p. 716), we see the same irregular features that are discussed in detail by Fort et al. (1986). The galaxy has been detected in H α (Boisson, Bottinelli & Gouguenheim, in preparation), with a total gas mass of $\sim 1.3 \times 10^9 \text{ M}_\odot$; the H α profile is double-peaked, suggesting that the gas is distributed in a ring. Spectra of the nuclear regions taken by Boisson et al. show no evidence for H α or N II emission. A ($B - I$) colour map constructed from our data (Fig. 15a, opposite p. 716) appears to show a faint

²It is possible that the knowledge that the larger ellipticals extend over most of a single CCD frame leads to an unconscious bias towards including only the lower 'sky' values in an average, and hence to an underestimate of the average sky-background in the frame. Observations on large telescopes, with the larger format CCDs currently available, should provide the final word on this matter.

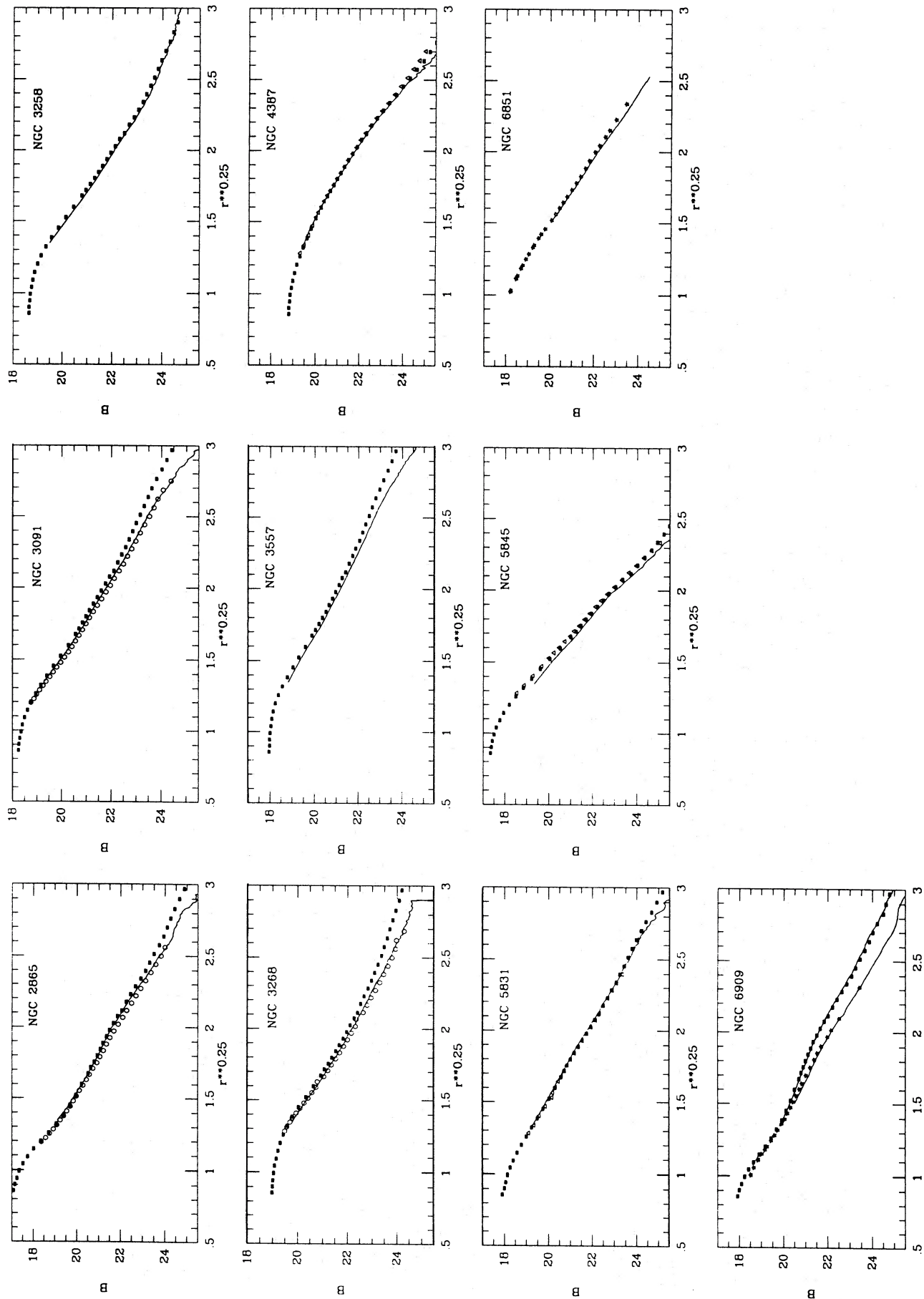


Figure 2. A comparison between the B -band photometry derived from our CCD data and previously published observations by Jedrzejewski (1987) (solid squares); Peletier et al. (1990) (open triangles; NGC 4387, 5831 and 5845); Jorgenson et al. (1992) (open circles; NGC 2865, 3091 and 3268) and Sparks et al. (1991) (stars; NGC 6851 and 6909). The last-mentioned comparisons match the mean profile, rather than the major-axis profile plotted in the other cases. Our NGC 5831 observations, obtained under non-photometric conditions, are scaled to match the 18.7 data at $r^{0.25} < 7$ and we have derived the NGC 4387 I -band photometry assuming $(R - V) = 0.07$ mag.

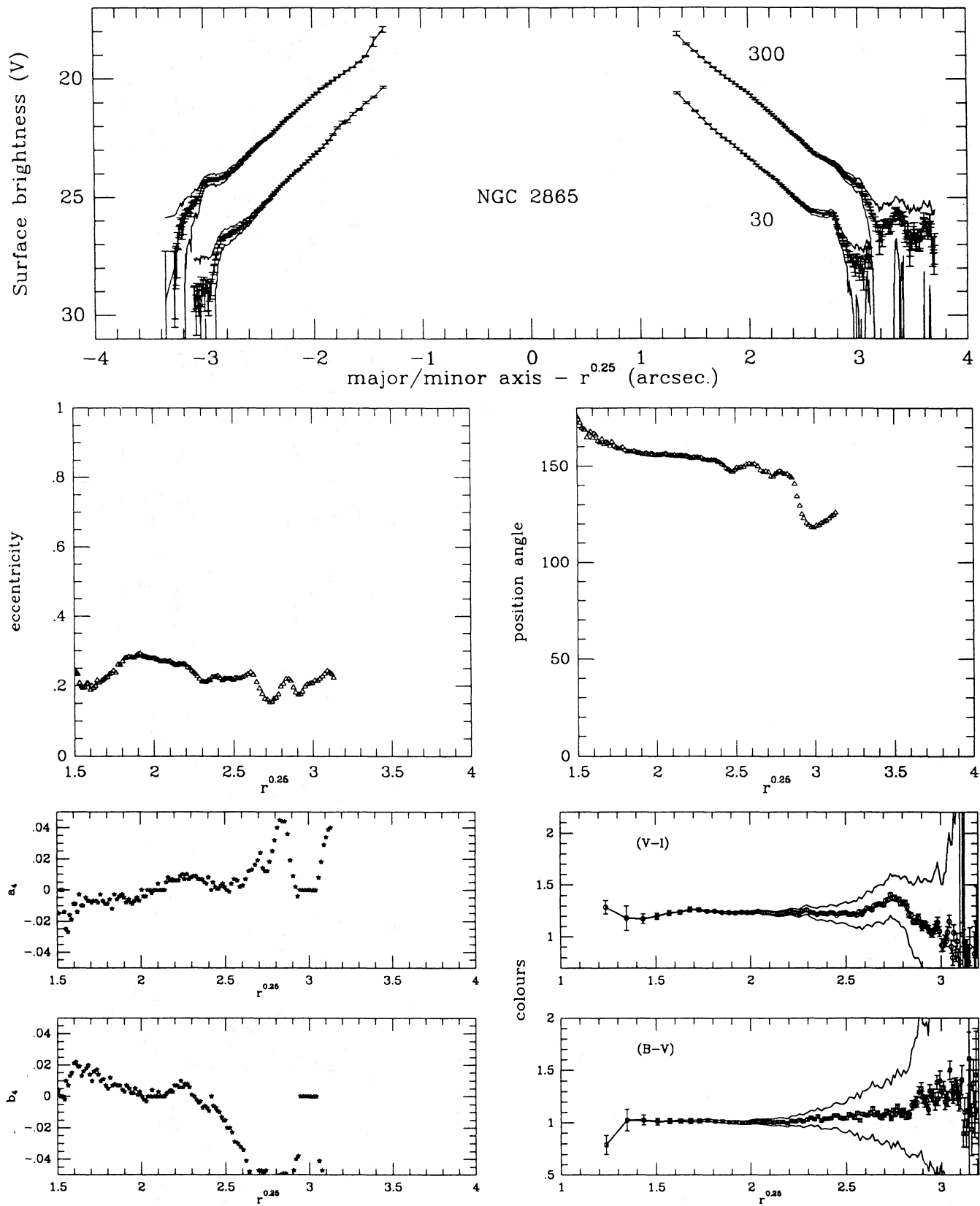


Figure 3. Results of our photometric analysis of NGC 2865. We plot both of the major- and minor-axis V -band photometric profiles in the uppermost panel. The labels give the position angles (measured north through east) of the positive profiles, and the minor-axis data are plotted with a zero-point offset by 2 mag. The error bars indicate the random (Poissonian) photometric uncertainties. We have also computed the effect of changing the sky-background level by ± 0.5 per cent, and the resultant profiles are shown – these are only distinguishable at large radii. The eccentricity, position angle (measured north through east), $\cos(4\theta)$ coefficient (a_4), and $\sin(4\theta)$ coefficient (b_4) (from PLEINPOR) are plotted. Finally, the lower right panels plot the $(B-V)$ and $(V-I)$ colours as a function of radius. The error bars show the formal uncertainty in the colour (based on photon statistics), while the upper and lower lines show the maximum effect of combining 0.5 per cent changes in the sky-background.

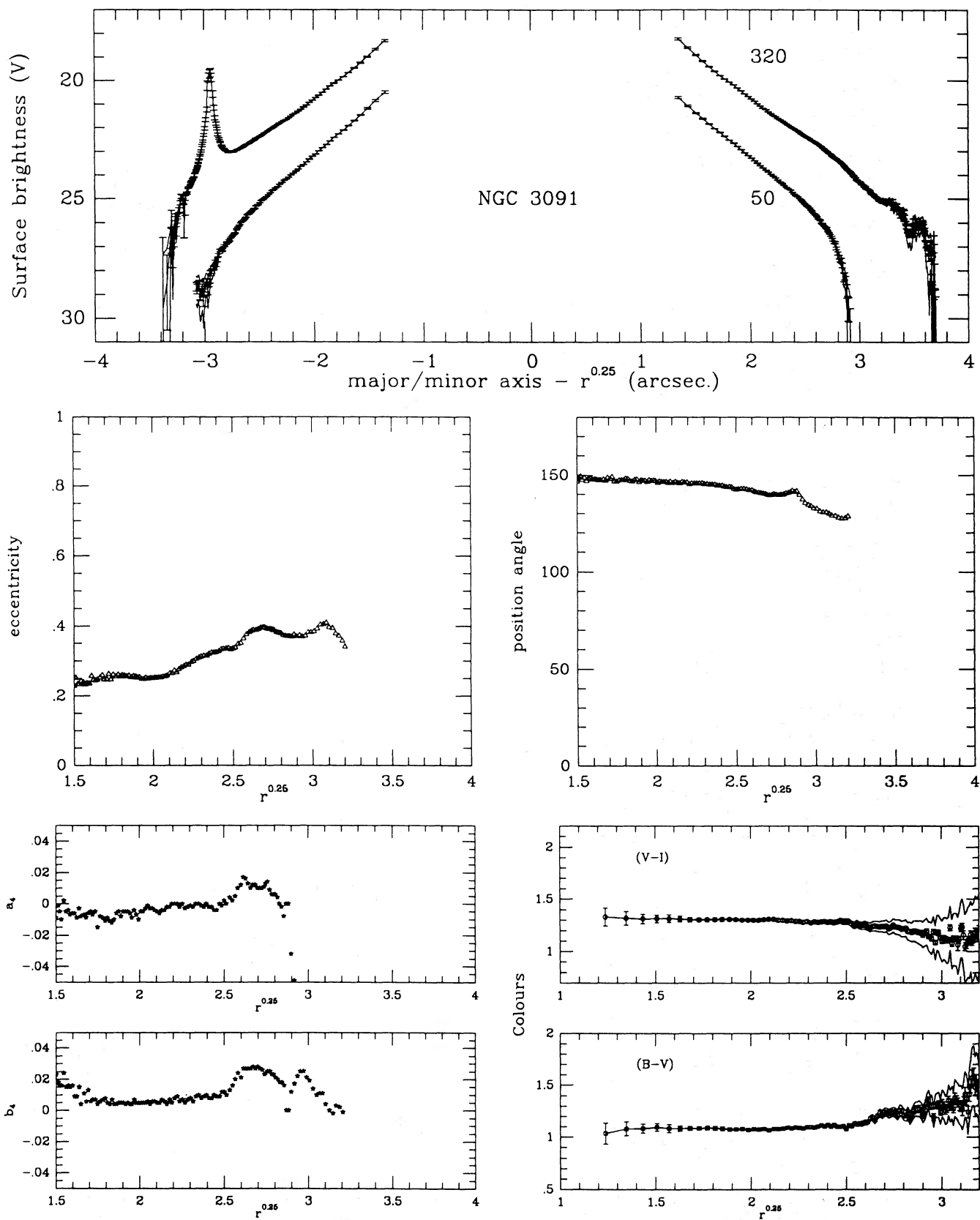


Figure 4. Photometric parameters for NGC 3091. The companion galaxy, NGC 3091A, is evident on the NW major-axis profile.

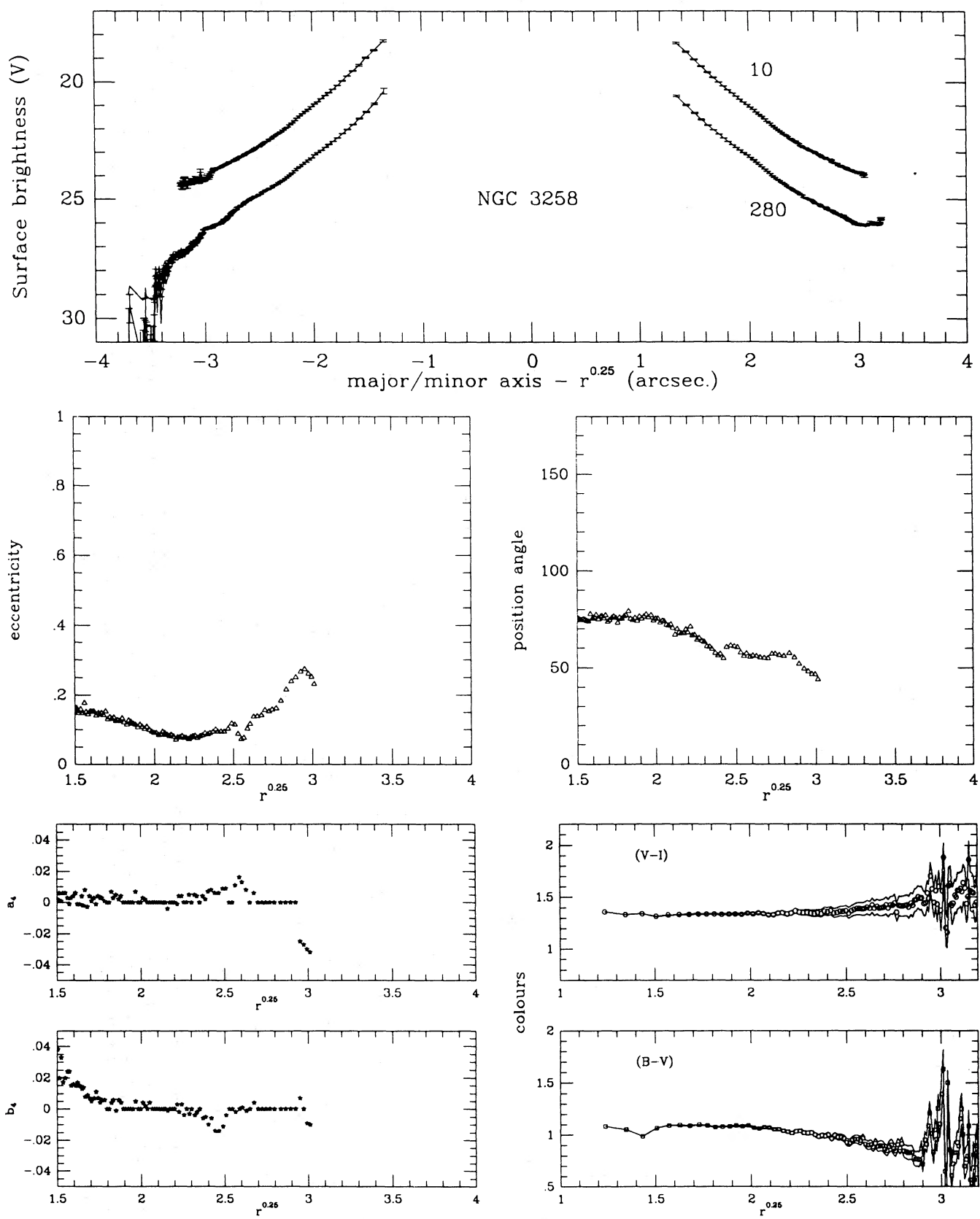


Figure 5. Photometric parameters for NGC 3258.

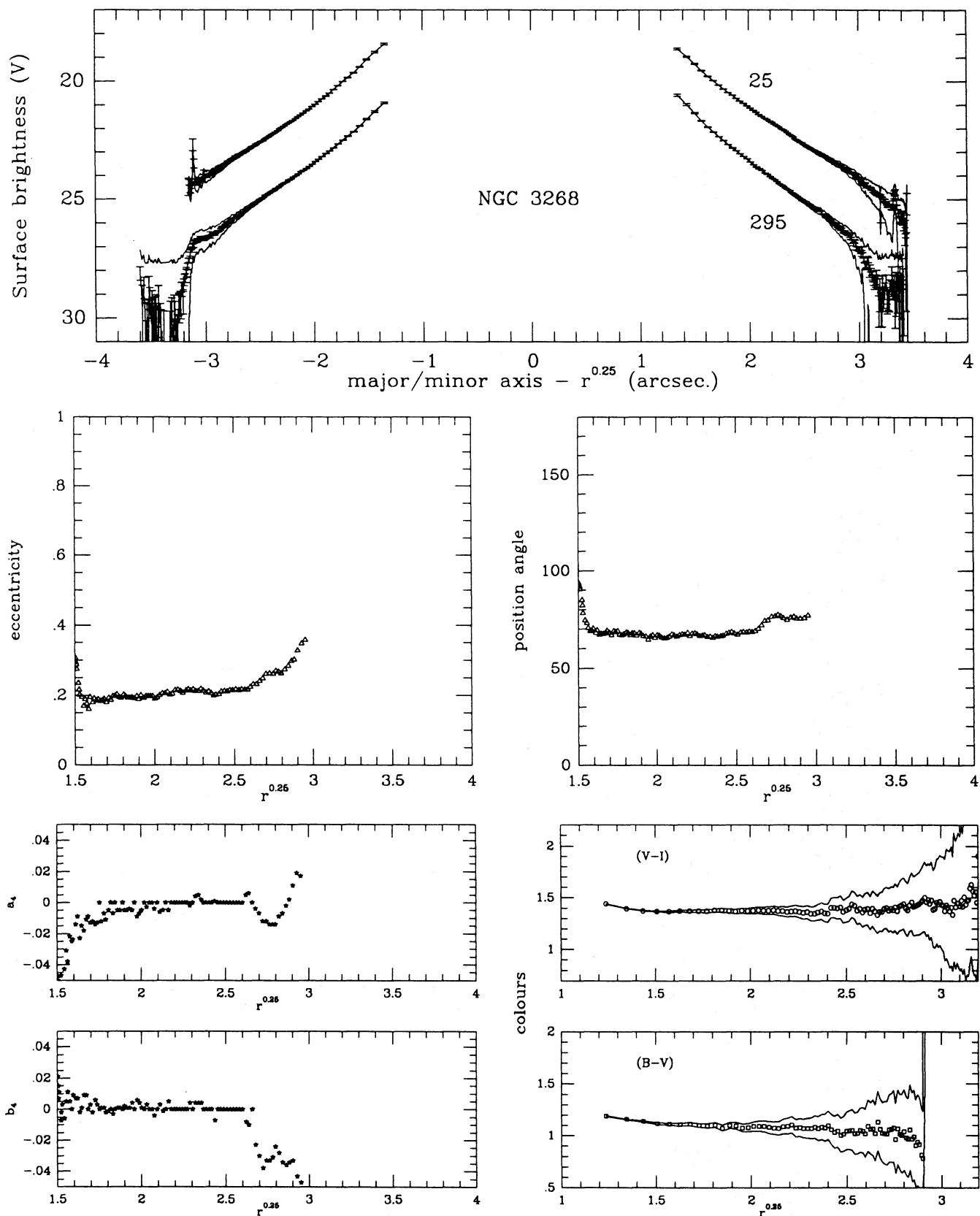


Figure 6. Photometric parameters for NGC 3268. A companion galaxy, NGC 3268A, probably accounts for the variations in the mean parameters at radii of 60 arcsec and above.

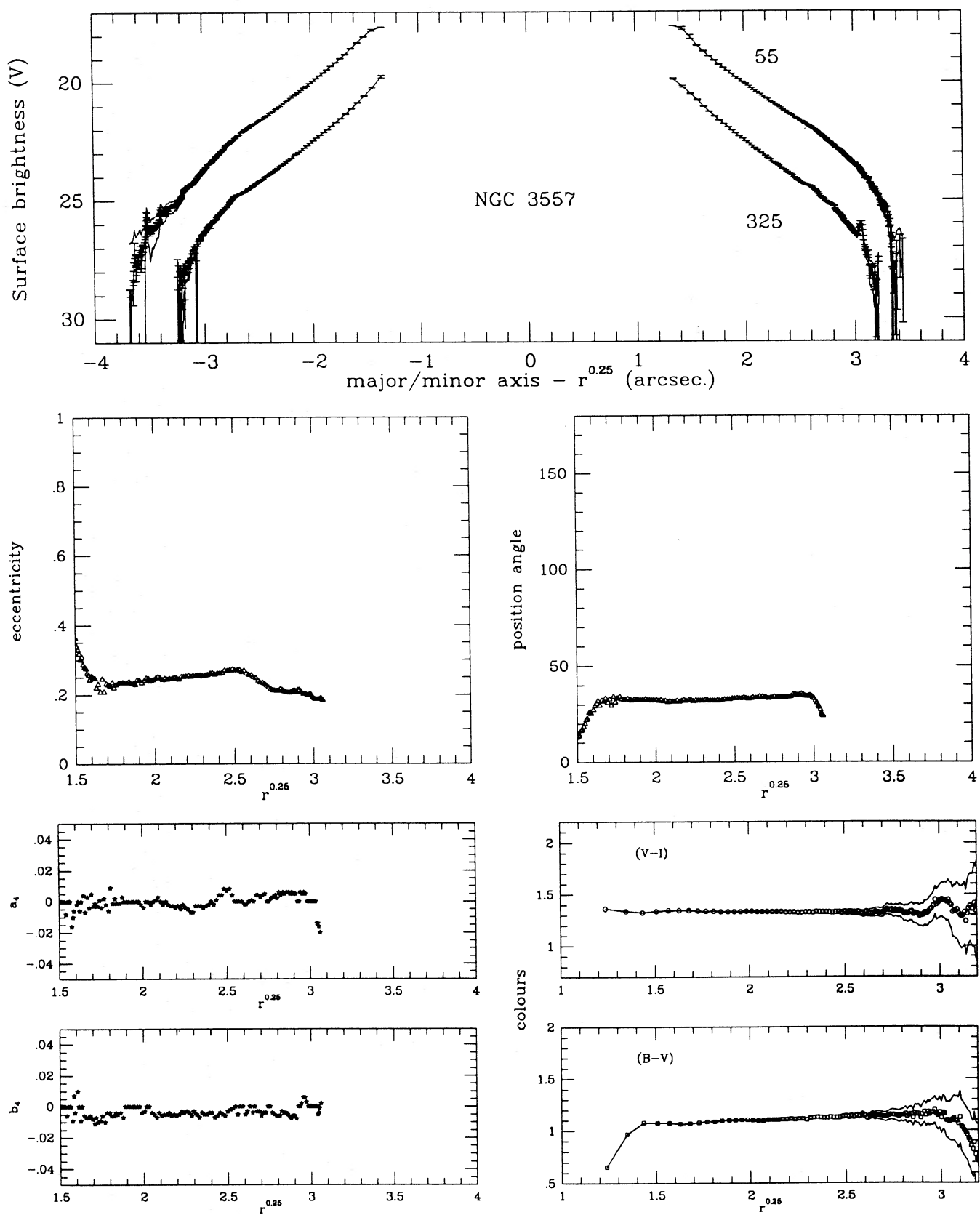


Figure 7. Photometric parameters for NGC 3557.

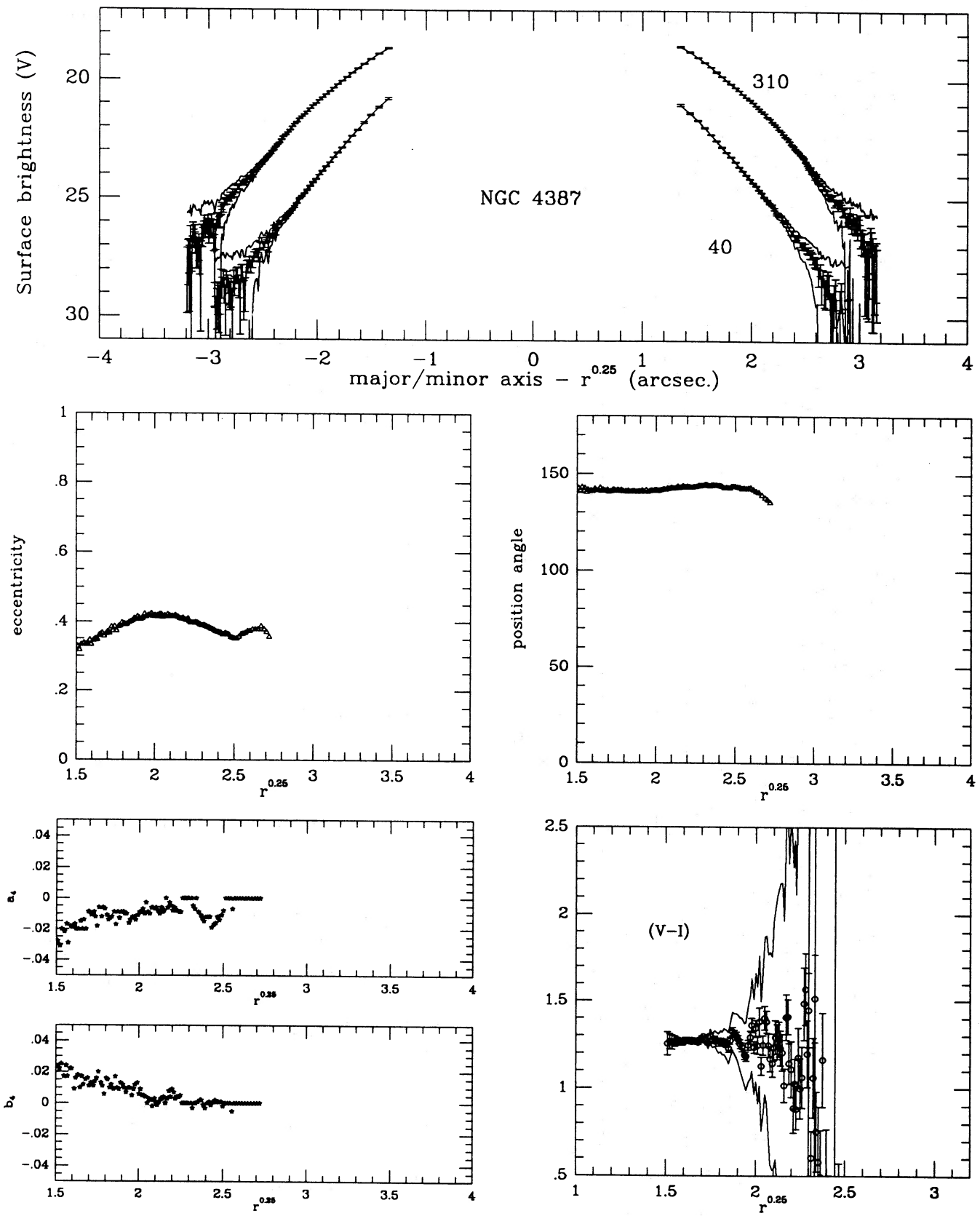


Figure 8. Photometric parameters for NGC 4387.

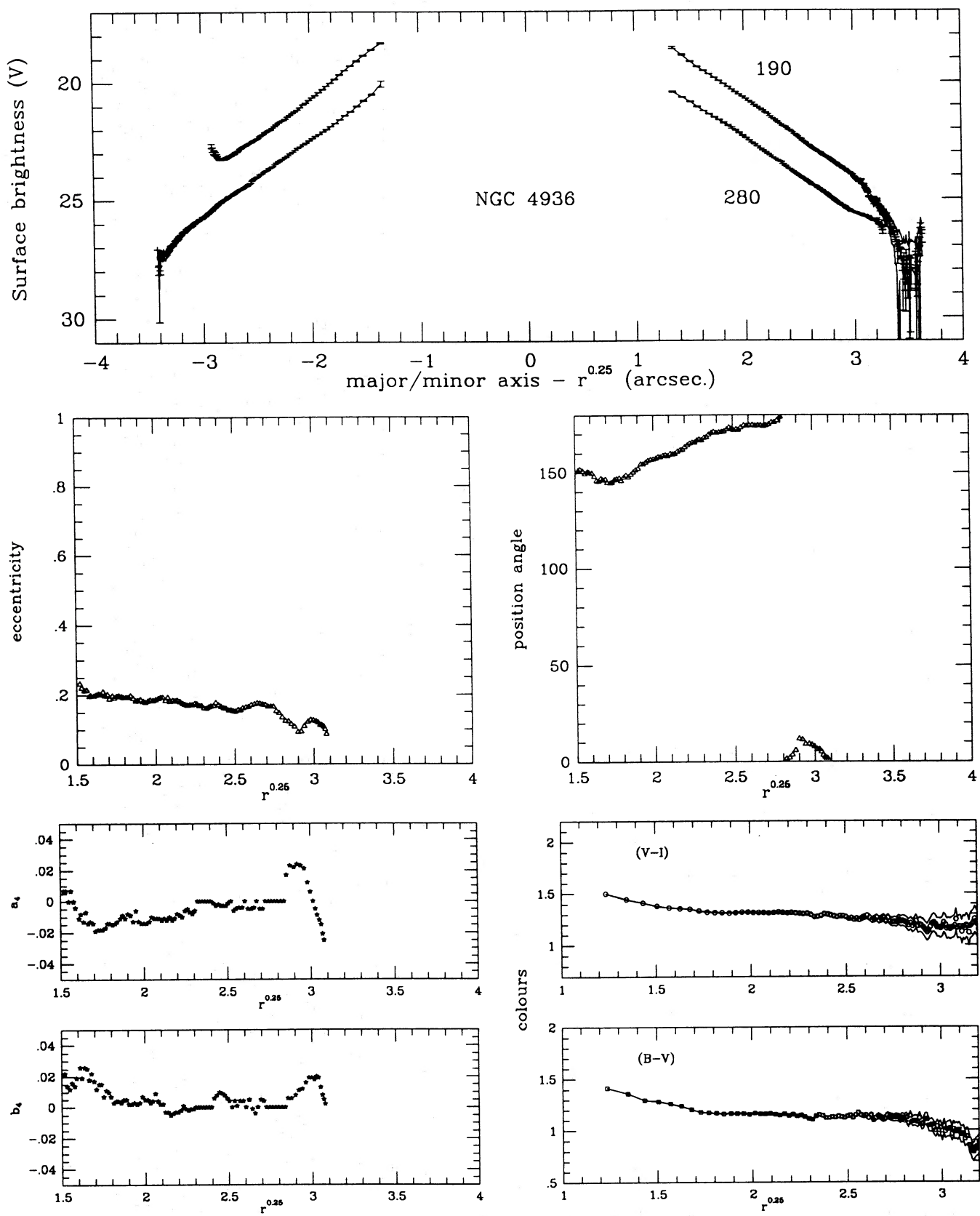


Figure 9. Photometric parameters for NGC 4936.

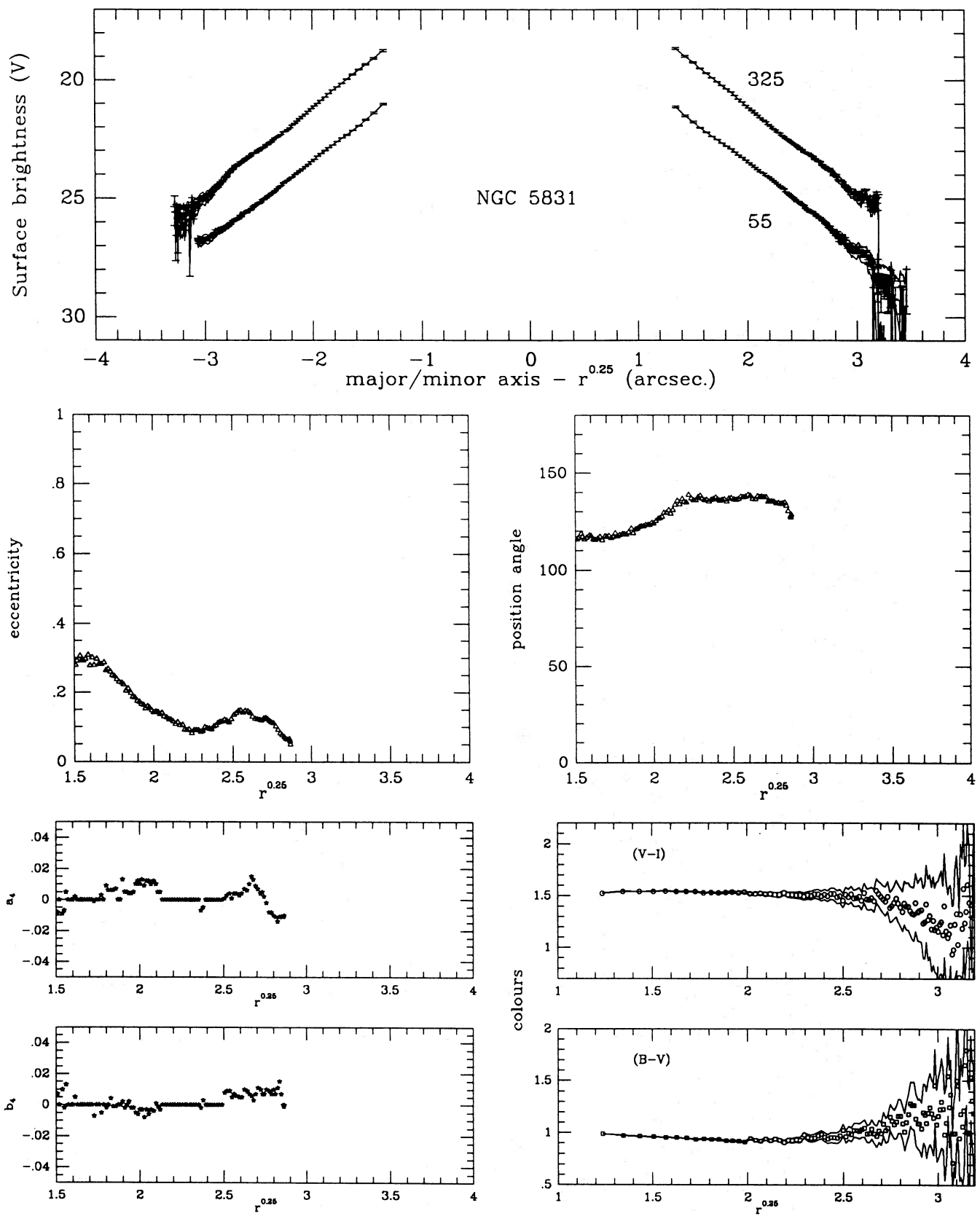


Figure 10. Photometric parameters for NGC 5831. The photometric zero-point of the major- and minor-axis profiles has been set using the J87 data.

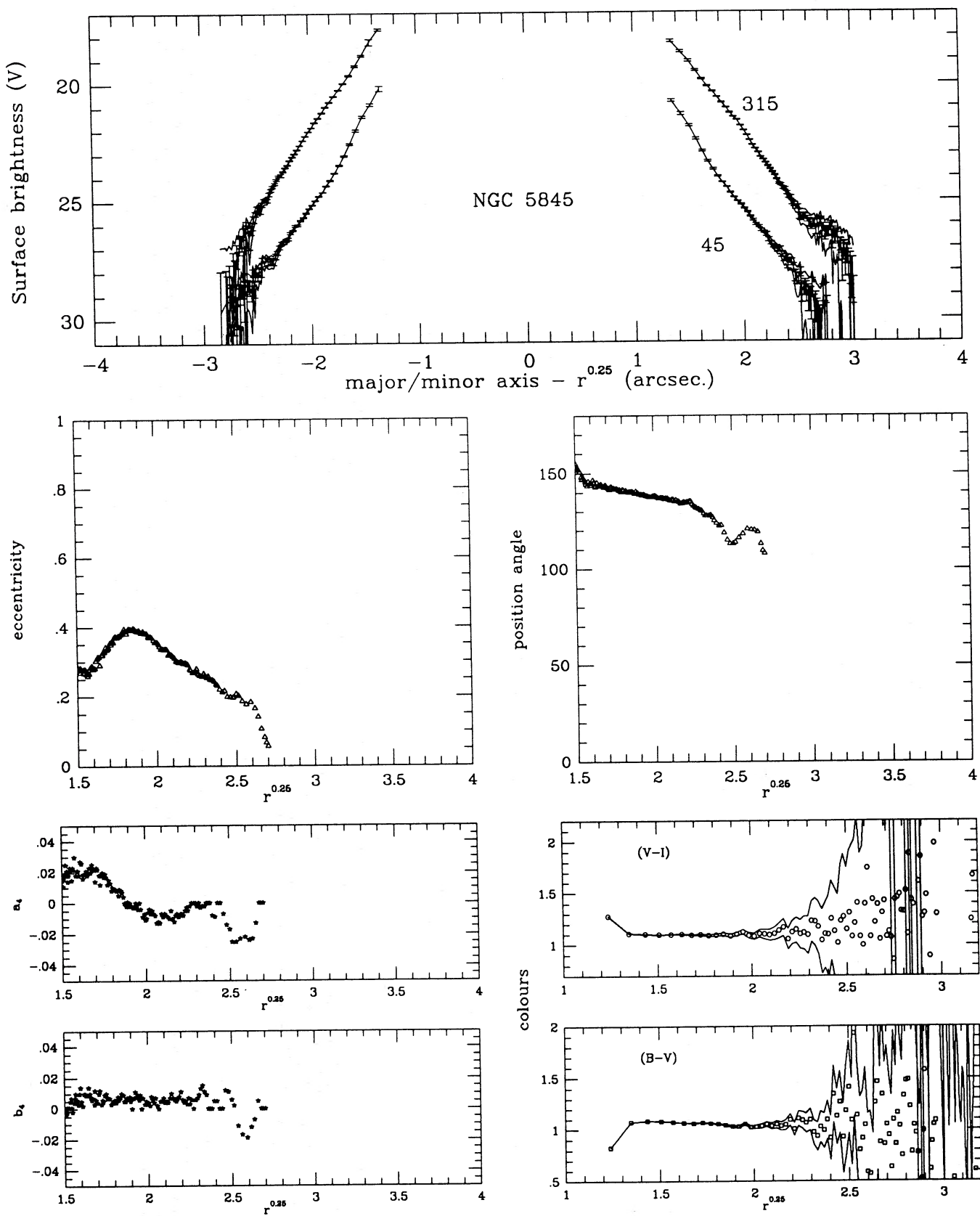


Figure 11. Photometric parameters for NGC 5845.

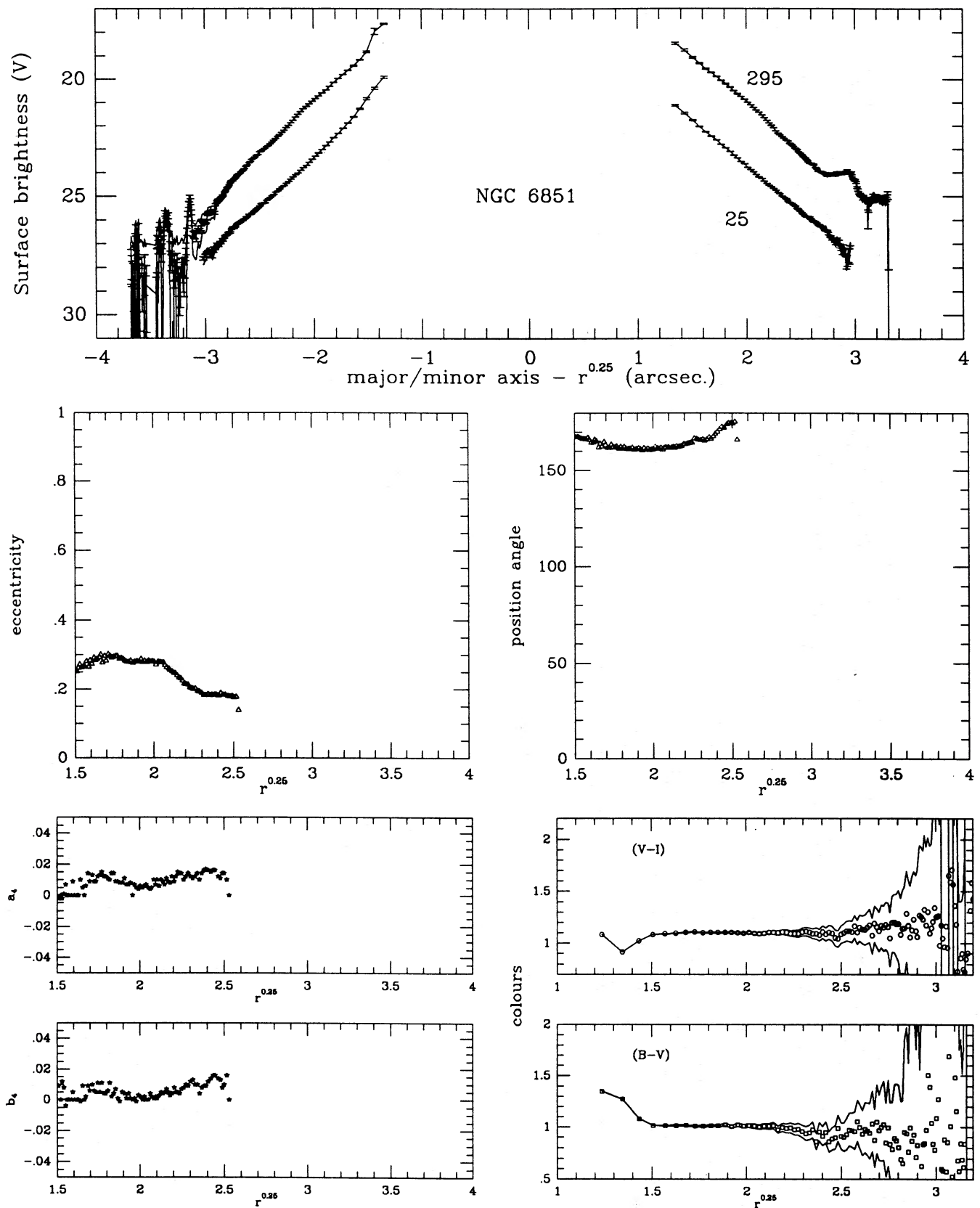


Figure 12. Photometric parameters for NGC 6851.

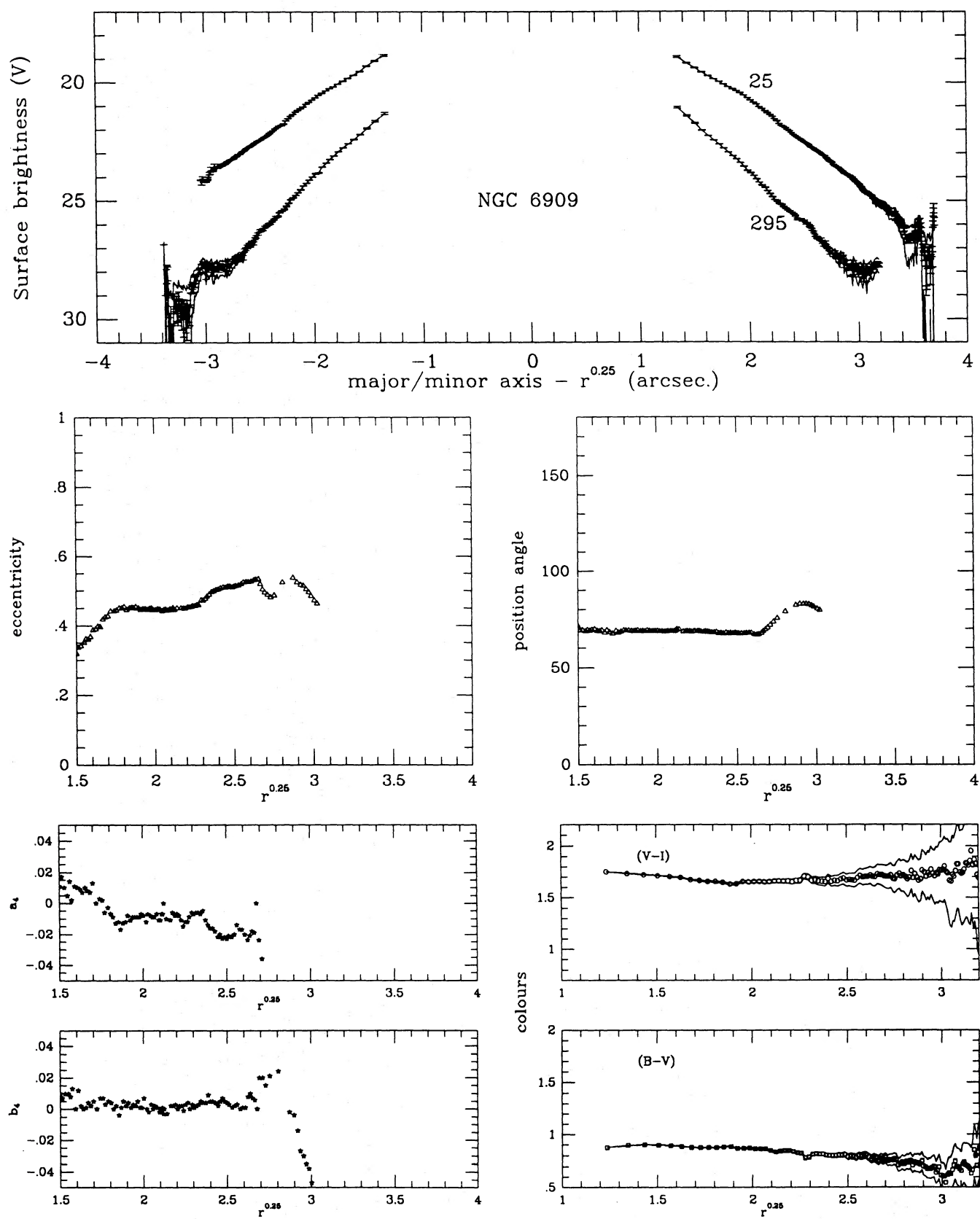


Figure 13. Photometric parameters for NGC 6909.

Table 4. Galactic characteristics. The colour gradients quoted above are computed as the average slope [against $\log(r)$] between radii of 4 and 40 arcsec, with a negative gradient implying a bluer colour at larger radii. Our observations show no significant colour gradients for any of these galaxies.

Galaxy	Environment	Morphology	Colour gradients
NGC 2865	Isolated; faint (+3 mag.) galaxies ~ 5' to SW	Shells ¹ ; boxy $r < 40''$ disky $r > 40''$	$\Delta_{B-R} \sim -0.05^2$ $\Delta_{B-R} = 0^3$
NGC 3091	loose group with 3072, 3085, 3096	shells, arcs boxy $r < 20''$	$\Delta_{B-R} = -0.01^2$ $\Delta_{B-R} = 0^3$
NGC 3258	2nd brightest galaxy moderately rich cluster	elliptical ($a_4, b_4=0$) 20° twist at $r=20''$ faint wisps to N, NW	$\Delta_{B-R} = 0.1^2$
NGC 3268	central cD moderately rich cluster	elliptical ($a_4, b_4=0$)	$\Delta_{B-R} = -0.15^2$ $\Delta_{B-R} = 0^3$
NGC 3557	isolated	pure elliptical	$\Delta_{B-R} = -0.01^2$ $\Delta_{Mg_2} = 0.02^4$
NGC 4387	Virgo cluster	boxy isophotes	$\Delta_{B-R} = 0.1^2$ $\Delta_{B-R} = -0.03^5$ $\Delta_{U-R} = -0.02^5$
NGC 4936	dominant member in moderately rich cluster	disturbed ¹ ; shells, double nucleus	
NGC 5831	NGC 5813 group	disky, $r < 20''$	$\Delta_{B-R} = -0.01^2$ $\Delta_{B-R} = -0.07^5$ $\Delta_{U-R} = -0.15^5$ $\Delta_{Mg_2} = -0.05^6$
NGC 5845	NGC 5813 group	disky, $r < 20''$ boxy, $r > 20''$	$\Delta_{B-R} = 0.1^2$ $\Delta_{B-R} = -0.07^5$ $\Delta_{U-R} = -0.04^5$ $\Delta_{Mg_2} = -0.05^6$
NGC 6851	NGC 6851A at 65"	disky, $r < 60''$ boxy, $r < 60''$	$\Delta_{B-V} = -0.15^7$ $\Delta_{V-I} = 0^7$
NGC 6909	isolated	boxy isophotes	$\Delta_{B-R} = -0.01^2$ none in BVI ⁷

References: ¹Malin & Carter (1980); ²Jedrzejewski (1987); ³Jorgenson et al. (1992); ⁴Carollo et al. (1993); ⁵Peletier et al. (1990); ⁶Gorgas et al. (1990); ⁷Sparks et al. (1991).

patch of extinction ~7 arcsec to the south-east of the nucleus, although no such feature was detected in Véron & Véron-Cetty's (1988) ($B-z$) map. Note that J87 find $(B-R)=1.6$ at $r=2$ arcsec, $(B-R)=1.8$ at $8 < r < 25$ arcsec and $(B-R)=1.6$ at $r=56$ arcsec.

NGC 3091. After subtracting our model from the observations, we see linear and arc-like residuals (Fig. 14b), also evident in the PA=320° profile (Fig. 4), which identify the system as a shell galaxy. The colour profiles at the same position angle show $(B-V)$ increasing, and $(V-I)$ decreasing, with radius for $r^{0.25} > 2.6$. This is physically implausible, and a more likely explanation is that we have underestimated $\Sigma_\nu(\text{sky})$ by 0.5 per cent (or by 2.5 adu). Unlike NGC 2865, neither nuclear emission due to ionized gas (Véron-Cetty & Véron 1986), nor H I (Boisson et al., in preparation) has been detected in this system.

NGC 3258. There is obvious wispy, low-surface-brightness structure to the north and north-west towards the edge of our CCD frame (at a distance of ~150 arcsec from the

nucleus). The lower luminosity elliptical, NGC 3260, lies ~4 arcmin from NGC 3258 in this direction, and it is possible that there is some tidal interaction. The $(B-V)$ colour becomes significantly bluer at $r \sim 50$ arcsec on the major axis, but there is no comparable effect in $(V-I)$, and we suspect a 1 per cent error in $\Sigma_\nu(\text{sky})$ to be the cause of the apparent colour change. Like the nearby NGC 3268, this galaxy has Hα and N II nuclear emission (in spectra taken by Boisson et al.). Roberts et al. (1991) cite an upper limit of 1.2 mJy to the H I 21-cm flux.

NGC 3268. NGC 3267, an S0/Sa system, lies only ~3 arcmin to the west, but there is no evidence for any interaction, although the nearer NGC 3268A, ~60 arcsec to the NE, may have a perturbing effect. There are no significant features on any of the colour maps.

NGC 3557. Despite the presence of a strong, double-tailed radio source, with a prominent central knot and a jet at a position angle of $78^\circ \pm 6^\circ$ (Birkinshaw & Davies 1985), this galaxy has the simplest optical structure (pure elliptical)

Table 5. NGC 2865.

$r^{0.25}$	Σ_V	ϵ	b_4	a_4	θ	$r^{0.25}$	Σ_V	ϵ	b_4	a_4	θ
1.505	18.95	0.24	175.4	-0.015	0.004	1.502	19.05	0.23	146.3	-0.009	0.023
1.543	19.16	0.20	168.9	-0.014	-0.002	1.546	19.25	0.24	148.4	0.002	0.024
1.588	19.36	0.21	167.7	-0.019	0.015	1.598	19.45	0.23	147.5	-0.006	0.016
1.633	19.56	0.20	162.9	-0.003	0.019	1.650	19.66	0.25	147.0	-0.003	0.004
1.683	19.76	0.22	162.1	-0.007	0.020	1.708	19.85	0.25	147.7	-0.005	0.006
1.735	19.96	0.24	160.6	-0.007	0.017	1.765	20.06	0.25	147.1	-0.008	0.005
1.775	20.11	0.26	158.9	-0.007	0.011	1.807	20.21	0.26	148.0	-0.009	0.005
1.816	20.26	0.28	157.3	-0.006	0.012	1.849	20.36	0.26	146.3	-0.010	0.004
1.859	20.41	0.28	157.6	-0.006	0.007	1.890	20.51	0.26	146.2	-0.003	0.005
1.900	20.57	0.29	156.6	-0.005	0.003	1.928	20.66	0.25	146.9	-0.005	0.005
1.940	20.71	0.28	156.3	-0.008	0.002	1.967	20.82	0.25	146.6	-0.004	0.007
1.978	20.86	0.28	156.1	-0.005	0.001	2.007	20.97	0.25	145.7	-0.005	0.005
2.016	21.02	0.28	155.4	-0.004	-0.002	2.048	21.12	0.25	146.2	-0.001	0.006
2.055	21.17	0.27	156.2	0.000	0.000	2.089	21.27	0.26	146.4	-0.004	0.006
2.100	21.32	0.27	155.3	0.000	0.000	2.132	21.43	0.27	145.8	-0.004	0.007
2.128	21.48	0.26	155.0	0.000	0.000	2.177	21.58	0.28	145.9	-0.002	0.007
2.162	21.63	0.26	155.2	0.008	0.003	2.222	21.73	0.29	145.4	0.000	0.009
2.197	21.78	0.26	154.7	0.006	0.007	2.269	21.89	0.31	145.6	-0.003	0.005
2.235	21.94	0.24	154.2	0.009	0.010	2.317	22.04	0.31	144.9	-0.002	0.006
2.271	22.09	0.23	154.1	0.010	0.008	2.366	22.20	0.32	144.9	-0.001	0.006
2.311	22.25	0.21	152.8	0.009	0.000	2.412	22.35	0.33	144.4	-0.002	0.008
2.338	22.36	0.22	152.7	0.007	-0.004	2.441	22.46	0.33	143.7	-0.004	0.010
2.364	22.46	0.22	152.9	0.007	-0.007	2.473	22.57	0.34	143.4	0.000	0.009
2.390	22.57	0.23	152.0	0.004	-0.007	2.500	22.67	0.34	142.2	0.002	0.012
2.416	22.68	0.22	150.8	0.000	0.000	2.533	22.78	0.35	142.8	0.004	0.013
2.441	22.78	0.22	148.7	0.002	-0.007	2.566	22.89	0.36	142.5	0.005	0.020
2.463	22.89	0.22	147.8	0.001	-0.010	2.600	23.00	0.38	142.0	0.012	0.021
2.487	23.00	0.22	147.0	0.004	-0.015	2.627	23.10	0.39	140.9	0.016	0.027
2.510	23.10	0.22	148.9	0.000	-0.020	2.656	23.22	0.39	140.4	0.010	0.027
2.538	23.22	0.22	149.2	0.004	-0.023	2.685	23.33	0.40	139.9	0.012	0.027
2.573	23.33	0.23	150.5	0.006	-0.030	2.710	23.44	0.39	139.2	0.010	0.027
2.606	23.44	0.24	150.6	0.003	-0.034	2.737	23.56	0.39	140.0	0.011	0.023
2.642	23.56	0.21	149.7	0.012	-0.048	2.757	23.67	0.39	139.5	0.014	0.025
2.678	23.67	0.18	146.9	0.016	-0.052	2.782	23.79	0.38	139.7	0.006	0.023
2.712	23.79	0.16	146.7	0.024	-0.047	2.803	23.91	0.38	139.9	0.006	0.021
2.739	23.91	0.15	144.3	0.012	-0.047	2.827	24.03	0.37	140.6	0.000	0.018
2.766	24.03	0.17	146.5	0.018	-0.052	2.854	24.16	0.37	141.7	-0.008	0.016
2.795	24.16	0.20	146.6	0.032	-0.056	2.881	24.29	0.38	141.6	0.000	0.000
2.828	24.29	0.22	145.7	0.045	-0.050	2.915	24.42	0.37	137.2	-0.049	0.017
2.857	24.42	0.21	143.9	0.044	-0.049	2.952	24.56	0.37	134.5	-0.069	0.025
2.888	24.56	0.18	134.2	0.019	-0.052	2.988	24.70	0.38	132.6	-0.072	0.021

Table 5. NGC 2865.**Table 6.** NGC 3091.

$r^{0.25}$	Σ_V	ϵ	b_4	a_4	θ	$r^{0.25}$	Σ_V	ϵ	b_4	a_4	θ
1.505	18.95	0.24	175.4	-0.015	0.004	1.502	19.05	0.23	146.3	-0.009	0.023
1.543	19.16	0.20	168.9	-0.014	-0.002	1.546	19.25	0.24	148.4	0.002	0.024
1.588	19.36	0.21	167.7	-0.019	0.015	1.598	19.45	0.23	147.5	-0.006	0.016
1.633	19.56	0.20	162.9	-0.003	0.019	1.650	19.66	0.25	147.0	-0.003	0.013
1.683	19.76	0.22	162.1	-0.007	0.020	1.708	19.85	0.25	147.7	-0.005	0.004
1.735	19.96	0.24	160.6	-0.007	0.017	1.765	20.06	0.25	147.1	-0.008	0.006
1.775	20.11	0.26	158.9	-0.007	0.011	1.807	20.21	0.26	148.0	-0.009	0.005
1.816	20.26	0.28	157.3	-0.006	0.012	1.849	20.36	0.26	146.3	-0.010	0.004
1.859	20.41	0.28	157.6	-0.006	0.007	1.890	20.51	0.26	146.2	-0.003	0.006
1.900	20.57	0.29	156.6	-0.005	0.003	1.928	20.66	0.25	146.9	-0.005	0.000
1.940	20.71	0.28	156.3	-0.008	0.002	1.967	20.82	0.25	146.6	-0.004	0.007
1.978	20.86	0.28	156.1	-0.005	0.001	2.007	20.97	0.25	145.7	-0.005	0.005
2.016	21.02	0.28	155.4	-0.004	-0.002	2.048	21.12	0.25	146.2	-0.001	0.006
2.055	21.17	0.27	156.2	0.000	0.000	2.089	21.27	0.26	146.4	-0.004	0.000
2.100	21.32	0.27	155.3	0.000	0.000	2.132	21.43	0.27	145.8	-0.004	0.000
2.128	21.48	0.26	155.0	0.000	0.000	2.177	21.58	0.28	145.9	-0.002	0.007
2.162	21.63	0.26	155.2	0.008	0.003	2.222	21.73	0.29	145.4	0.000	0.009
2.197	21.78	0.26	154.7	0.006	0.007	2.269	21.89	0.31	145.6	-0.003	0.005
2.235	21.94	0.24	154.2	0.009	0.010	2.317	22.04	0.31	144.9	-0.002	0.006
2.271	22.09	0.23	154.1	0.010	0.008	2.366	22.20	0.32	144.9	-0.001	0.006
2.311	22.25	0.21	152.8	0.009	0.000	2.412	22.35	0.33	144.4	-0.002	0.008
2.338	22.36	0.22	152.7	0.007	-0.004	2.441	22.46	0.33	143.7	-0.004	0.010
2.364	22.46	0.22	152.9	0.007	-0.007	2.473	22.57	0.34	143.4	0.000	0.009
2.390	22.57	0.23	152.0	0.004	-0.007	2.500	22.67	0.34	142.2	0.002	0.012
2.416	22.68	0.22	150.8	0.000	0.000	2.533	22.78	0.35	142.8	0.004	0.013
2.441	22.78	0.22	148.7	0.002	-0.007	2.566	22.89	0.36	142.5	0.005	0.020
2.463	22.89	0.22	147.8	0.001	-0.010	2.600	23.00	0.38	142.0	0.012	0.021
2.487	23.00	0.22	147.0	0.004	-0.015	2.627	23.10	0.39	140.9	0.016	0.027
2.510	23.10	0.22	148.9	0.000	-0.020	2.656	23.22	0.39	140.4	0.010	0.027
2.538	23.22	0.22	149.2	0.004	-0.023	2.685	23.33	0.40	139.9	0.012	0.027
2.573	23.33	0.23	150.5	0.006	-0.030	2.710	23.44	0.39	139.2	0.010	0.027
2.606	23.44	0.24	150.6	0.003	-0.034	2.737	23.56	0.39	140.0	0.011	0.023
2.642	23.56	0.21	149.7	0.012	-0.048	2.757	23.67	0.39	139.5	0.014	0.025
2.678	23.67	0.18	146.9	0.016	-0.052	2.782	23.79	0.38	139.7	0.006	0.023
2.712	23.79	0.16	146.7	0.024	-0.047	2.803	23.91	0.38	139.9	0.006	0.021
2.739	23.91	0.15	144.3	0.012	-0.047	2.827	24.03	0.37	140.6	0.000	0.018
2.766	24.03	0.17	146.5	0.018	-0.052	2.854	24.16	0.37	141.7	-0.008	0.016
2.795	24.16	0.20	146.6	0.032	-0.056	2.881	24.29	0.38	141.6	0.000	0.000
2.828	24.29	0.22	145.7	0.045	-0.050	2.915	24.42	0.37	137.2	-0.049	0.017
2.857	24.42	0.21	143.9	0.044	-0.049	2.952	24.56	0.37	134.5	-0.069	0.025
2.888	24.56	0.18	134.2	0.019	-0.052	2.988	24.70	0.38	132.6	-0.072	0.021

Table 7. NGC 3258.
$r^{0.25}$	Σ_V	ϵ	b_4	a_4	θ </th

Table 8. NGC 3268.

$r^{0.25}$	Σ_V	ϵ	a_4	b_4	θ						
1.503	19.10	0.31	93.6	-0.047	0.021	1.501	18.10	0.36	12.8	0.000	1.510
1.523	19.31	0.23	84.8	-0.047	-0.007	1.532	18.30	0.30	16.7	0.000	1.562
1.555	19.51	0.17	73.0	-0.031	0.005	1.566	18.50	0.28	22.4	0.000	1.611
1.596	19.70	0.19	70.3	-0.024	0.009	1.605	18.71	0.25	27.2	-0.002	1.656
1.647	19.91	0.19	67.4	-0.015	0.001	1.645	18.91	0.23	29.6	0.004	1.701
1.698	20.11	0.18	68.3	-0.013	0.003	1.695	19.10	0.23	31.0	0.005	1.747
1.737	20.26	0.20	68.3	-0.013	0.003	1.731	19.25	0.23	34.2	-0.003	1.781
2.041	20.41	0.19	66.9	-0.007	0.001	1.771	19.41	0.23	34.1	-0.010	1.814
2.178	20.56	0.20	68.0	0.000	0.000	1.807	19.56	0.23	32.5	0.002	1.849
1.818	20.71	0.19	67.7	-0.005	0.001	1.846	19.70	0.23	32.1	-0.001	1.881
1.858	20.86	0.19	67.5	-0.005	0.002	1.889	19.86	0.24	32.4	0.000	1.912
1.901	21.02	0.20	64.6	-0.005	0.004	1.934	20.01	0.24	32.9	0.000	1.946
1.946	21.17	0.20	65.5	-0.007	0.004	1.975	20.16	0.24	32.1	0.000	1.979
1.988	21.32	0.20	65.7	-0.003	0.003	2.019	20.31	0.25	31.8	0.000	2.010
2.032	21.48	0.21	66.0	-0.004	-0.004	2.062	20.46	0.25	31.8	0.000	2.041
2.128	21.63	0.21	66.0	-0.005	-0.001	2.107	20.61	0.25	31.5	0.000	2.071
2.177	21.78	0.21	67.1	0.000	0.000	2.150	20.76	0.24	31.4	-0.002	2.100
2.225	21.94	0.21	67.6	0.000	0.000	2.194	20.92	0.25	31.9	-0.004	2.131
2.273	22.09	0.21	66.4	0.000	0.000	2.240	21.07	0.25	31.5	-0.002	2.158
2.320	22.25	0.21	65.9	0.004	0.004	2.284	21.22	0.25	32.0	-0.007	2.187
2.370	22.41	0.20	66.4	0.000	0.000	2.330	21.37	0.26	32.0	-0.003	2.218
2.403	22.51	0.20	66.4	0.000	0.000	2.362	21.48	0.26	31.8	-0.004	2.259
2.437	22.62	0.21	67.6	0.001	-0.007	2.392	21.58	0.26	32.2	-0.002	2.295
2.471	22.73	0.21	68.5	0.000	0.000	2.423	21.68	0.26	32.3	-0.002	2.278
2.509	22.83	0.22	67.2	0.000	0.000	2.454	21.78	0.27	32.5	0.004	2.307
2.547	22.94	0.22	68.3	0.000	0.000	2.486	21.89	0.27	33.1	0.008	2.341
2.583	23.05	0.22	68.7	0.000	0.000	2.517	21.99	0.27	33.3	-0.002	2.370
2.621	23.16	0.23	68.9	0.005	-0.008	2.547	22.09	0.26	33.0	0.000	2.395
2.660	23.27	0.24	71.8	0.000	0.000	2.575	22.20	0.26	33.0	0.000	2.385
2.701	23.38	0.26	74.4	-0.007	-0.030	2.605	22.30	0.26	32.9	-0.002	2.408
2.744	23.50	0.26	76.5	-0.012	-0.033	2.633	22.41	0.25	33.2	0.000	2.430
2.780	23.61	0.27	76.6	-0.014	-0.031	2.661	22.51	0.23	34.1	0.000	2.456
2.819	23.73	0.27	74.6	-0.009	-0.028	2.687	22.62	0.23	33.6	0.004	2.477
2.863	23.85	0.30	76.2	-0.002	-0.036	2.714	22.73	0.22	33.1	0.004	2.501
2.903	23.96	0.33	75.3	0.011	-0.033	2.740	22.83	0.21	33.3	0.000	2.530

Table 9. NGC 3557.

$r^{0.25}$	Σ_V	ϵ	a_4	b_4	θ						
1.501	18.10	0.36	12.8	0.000	1.501	18.10	0.36	12.8	0.000	1.510	19.71
1.523	18.30	0.30	16.7	0.000	1.532	18.30	0.30	16.7	0.000	1.562	19.91
1.555	18.50	0.28	22.4	0.000	1.566	18.50	0.28	22.4	0.000	1.611	20.11
1.596	18.71	0.25	27.2	-0.010	1.605	18.71	0.25	27.2	-0.002	1.656	20.31
1.647	18.91	0.23	29.6	0.004	1.645	18.91	0.23	29.6	0.006	1.701	20.51
1.698	19.10	0.23	31.0	0.005	1.695	19.10	0.23	31.0	0.008	1.747	20.72
1.737	19.25	0.23	34.2	-0.010	1.731	19.25	0.23	34.2	-0.010	1.781	20.87
2.041	19.41	0.23	34.1	0.002	1.771	19.41	0.23	34.1	0.002	1.814	20.92
2.178	19.56	0.23	32.5	0.009	1.807	19.56	0.23	32.5	0.006	1.849	21.17
1.818	19.70	0.20	68.0	0.000	0.000	1.846	19.70	0.23	32.1	-0.005	1.881
1.858	19.86	0.19	67.7	-0.005	0.001	1.889	19.86	0.24	32.4	0.000	1.912
1.901	19.91	0.19	67.5	-0.005	0.002	1.934	20.01	0.24	32.9	0.000	1.946
1.946	20.01	0.20	64.6	-0.005	0.004	1.975	20.16	0.24	32.1	0.000	1.979
1.988	20.17	0.20	65.5	-0.007	0.004	2.019	20.31	0.25	31.8	0.000	2.010
2.032	20.32	0.20	65.7	-0.003	0.003	2.062	20.46	0.25	31.5	0.000	2.041
2.128	20.48	0.21	66.0	-0.004	-0.004	2.107	20.61	0.25	31.5	0.000	2.071
2.177	20.63	0.21	66.0	-0.005	-0.001	2.150	20.76	0.24	31.4	-0.002	2.100
2.225	20.78	0.21	67.1	0.000	0.000	2.194	20.92	0.25	31.9	-0.004	2.131
2.273	20.94	0.21	67.6	0.000	0.000	2.240	21.07	0.25	31.5	-0.002	2.158
2.320	21.17	0.21	66.4	-0.004	0.004	2.284	21.22	0.25	32.0	-0.007	2.187
2.370	21.32	0.20	66.4	0.000	0.000	2.330	21.37	0.26	32.0	-0.003	2.218
2.403	21.48	0.20	66.4	0.000	0.000	2.362	21.48	0.26	31.8	-0.004	2.259
2.437	21.63	0.21	67.6	0.001	-0.007	2.392	21.58	0.26	32.2	-0.002	2.295
2.471	21.78	0.21	68.5	0.000	0.000	2.423	21.68	0.26	32.3	-0.002	2.278
2.509	21.94	0.21	67.2	0.000	0.000	2.454	21.78	0.27	32.5	0.004	2.307
2.547	22.10	0.20	68.3	0.000	0.000	2.486	21.89	0.27	33.1	0.008	2.341
2.583	22.25	0.22	68.7	0.000	0.000	2.517	21.99	0.27	33.3	-0.002	2.370
2.621	22.41	0.22	68.9	0.005	-0.008	2.547	22.09	0.26	33.0	0.000	2.395
2.660	22.56	0.24	71.8	0.000	0.000	2.575	22.20	0.26	33.0	0.000	2.385
2.701	22.72	0.26	74.4	-0.007	-0.030	2.605	22.30	0.26	32.9	-0.002	2.408
2.744	22.88	0.26	76.5	-0.012	-0.033	2.633	22.41	0.25	33.2	0.000	2.430
2.780	23.05	0.27	76.6	-0.014	-0.031	2.661	22.51	0.23	34.1	0.000	2.456
2.819	23.16	0.27	74.6	-0.009	-0.028	2.687	22.62	0.23	33.6	0.004	2.477
2.863	23.27	0.30	76.2	-0.002	-0.036	2.714	22.73	0.22	33.1	0.004	2.501
2.903	23.38	0.33	75.3	0.011	-0.033	2.740	22.83	0.21	33.3	0.000	2.530

Table 10. NGC 4387.

$r^{0.25}$	Σ_V	ϵ	a_4	b_4	θ						
1.501	18.10	0.36	12.8	0.000	1.501	18.10	0.36	12.8	0.000	1.510	19.71
1.523	18.30	0.30	16.7	0.000	1.532	18.30	0.30	16.7	0.000	1.562	19.91
1.555	18.50	0.28	22.4	0.000	1.566	18.50	0.28	22.4	0.000	1.611	20.11
1.596	18.71	0.25	27.2	-0.002	1.605	18.71	0.25	27.2	-0.002	1.656	20.31
1.647	18.91	0.23	29.6	0.004	1.645	18.91	0.23	29.6	0.006	1.701	20.51
1.698	19.10	0.23	31.0	0.005	1.695	19.10	0.23	31.0	0.008	1.747	20.72
1.737	19.25	0.23	34.2	-0.010	1.731	19.25	0.23	34.2	-0.010	1.781	20.87
2.041	19.41	0.23	34.1	0.002	1.771	19.41	0.23	34.1	0.002	1.814	20.92
2.178	19.56	0.23	32.5	0.009	1.807	19.56	0.23	32.5	0.006	1.849	21.17
1.818	19.70	0.20	68.0	0.000	0.000	1.846	19.70	0.23	32.1	-0.005	1.881
1.858	19.86	0.19	67.7	-0.005	0.001	1.889	19.				

Table 11. NGC 4936.

$r^{0.25}$	Σ_V	ϵ	a_4	b_4	θ	$r^{0.25}$	Σ_V	ϵ	a_4	b_4	θ
1.520	18.90	0.23	151.0	0.007	0.022	1.509	19.95	0.28	115.6	-0.008	0.007
1.580	19.11	0.20	150.5	0.000	0.014	1.559	20.16	0.29	115.6	0.005	0.013
1.639	19.31	0.20	145.8	-0.013	0.026	1.615	20.36	0.30	115.7	0.002	0.005
1.695	19.50	0.20	146.5	-0.014	0.017	1.671	20.56	0.28	115.2	0.000	0.000
1.752	19.71	0.20	146.2	-0.018	0.007	1.728	20.76	0.26	116.3	-0.001	-0.007
1.811	19.91	0.19	147.6	-0.015	0.003	1.784	20.97	0.23	117.9	0.000	0.000
1.856	20.06	0.19	149.0	-0.011	0.003	1.826	21.12	0.20	118.1	0.006	0.004
1.902	20.21	0.19	152.0	-0.008	0.002	1.869	21.27	0.19	118.8	0.000	0.000
1.951	20.36	0.18	155.2	-0.006	0.002	1.910	21.42	0.17	122.2	0.005	-0.002
1.999	20.51	0.19	156.8	-0.014	0.005	1.948	21.58	0.15	123.0	0.004	-0.002
2.046	20.66	0.19	158.1	-0.010	0.004	1.988	21.73	0.15	124.2	0.012	-0.006
2.091	20.82	0.18	158.6	-0.011	0.002	2.027	21.89	0.14	126.4	0.009	-0.008
2.136	20.97	0.18	159.7	-0.012	-0.003	2.066	22.04	0.13	129.2	0.010	-0.003
2.184	21.12	0.17	161.8	-0.011	-0.003	2.108	22.20	0.12	128.8	0.005	-0.001
2.229	21.27	0.17	165.0	-0.010	0.001	2.151	22.36	0.11	135.5	0.000	0.000
2.275	21.42	0.17	166.5	-0.007	-0.001	2.193	22.51	0.09	135.1	0.000	0.000
2.320	21.58	0.16	167.9	0.000	0.000	2.238	22.67	0.08	136.7	0.000	0.000
2.367	21.73	0.17	170.4	0.000	0.000	2.280	22.83	0.09	137.5	0.000	0.000
2.415	21.89	0.17	170.7	-0.001	0.006	2.321	23.00	0.10	135.9	0.000	0.000
2.463	22.04	0.16	172.3	-0.003	0.009	2.364	23.16	0.09	136.1	-0.007	-0.002
2.507	22.20	0.15	171.8	-0.001	0.004	2.404	23.33	0.11	136.1	0.000	0.000
2.538	22.30	0.16	172.0	-0.006	0.004	2.432	23.44	0.12	136.1	0.000	0.000
2.572	22.41	0.16	174.3	-0.004	0.004	2.461	23.56	0.12	135.2	0.000	0.000
2.606	22.51	0.17	174.3	0.000	0.000	2.489	23.67	0.12	137.0	0.000	0.000
2.644	22.62	0.18	174.3	-0.005	-0.001	2.521	23.79	0.14	135.9	0.003	0.009
2.677	22.72	0.17	174.5	0.000	0.000	2.550	23.91	0.15	137.5	0.001	0.005
2.712	22.83	0.17	174.4	-0.005	0.004	2.577	24.03	0.15	137.5	0.004	0.006
2.745	22.94	0.17	176.1	0.000	0.000	2.609	24.16	0.14	138.0	0.004	0.005
2.780	23.05	0.15	176.9	0.000	0.000	2.641	24.29	0.12	136.1	0.006	0.009
2.818	23.16	0.12	174.3	0.000	0.000	2.668	24.42	0.12	137.4	0.015	0.006
2.855	23.27	0.12	173.3	0.017	0.006	2.693	24.56	0.12	137.4	0.009	0.007
2.900	23.38	0.09	11.8	0.022	0.008	2.721	24.70	0.12	135.0	0.004	0.010
2.940	23.50	0.11	8.9	0.023	0.012	2.743	24.84	0.11	135.3	0.002	0.007
2.980	23.61	0.13	8.4	0.012	0.019	2.772	25.00	0.10	134.1	-0.008	0.009
2.818	23.16	0.12	1.3	0.000	0.000	2.799	25.16	0.08	134.0	-0.010	0.010
2.824	23.27	0.12	3.3	0.017	0.006	2.824	25.33	0.07	134.6	-0.014	0.011
2.846	23.38	0.09	11.8	0.022	0.008	2.851	25.51	0.06	130.1	-0.011	0.007
2.863	23.50	0.11	8.9	0.023	0.012	2.743	25.72	0.06	127.0	-0.011	0.001
2.869	23.61	0.13	8.4	0.012	0.019	2.772	25.00	0.10	134.1	-0.011	0.001
2.873	23.16	0.12	1.3	0.000	0.000	2.799	25.16	0.08	134.0	-0.010	0.010
2.877	23.27	0.12	3.3	0.017	0.006	2.824	25.33	0.07	134.6	-0.014	0.011
2.886	23.38	0.09	11.8	0.022	0.008	2.846	25.51	0.06	130.1	-0.011	0.007
2.890	23.50	0.11	8.9	0.023	0.012	2.743	25.72	0.06	127.0	-0.011	0.001
2.894	23.61	0.13	8.4	0.012	0.019	2.772	25.00	0.10	134.1	-0.011	0.001
2.877	23.16	0.12	1.3	0.000	0.000	2.799	25.16	0.08	134.0	-0.010	0.010
2.886	23.27	0.12	3.3	0.017	0.006	2.824	25.33	0.07	134.6	-0.014	0.011
2.890	23.38	0.09	11.8	0.022	0.008	2.846	25.51	0.06	130.1	-0.011	0.007
2.894	23.50	0.11	8.9	0.023	0.012	2.743	25.72	0.06	127.0	-0.011	0.001
2.898	23.61	0.13	8.4	0.012	0.019	2.772	25.00	0.10	134.1	-0.011	0.001
2.877	23.16	0.12	1.3	0.000	0.000	2.799	25.16	0.08	134.0	-0.010	0.010
2.886	23.27	0.12	3.3	0.017	0.006	2.824	25.33	0.07	134.6	-0.014	0.011
2.890	23.38	0.09	11.8	0.022	0.008	2.846	25.51	0.06	130.1	-0.011	0.007
2.894	23.50	0.11	8.9	0.023	0.012	2.743	25.72	0.06	127.0	-0.011	0.001
2.898	23.61	0.13	8.4	0.012	0.019	2.772	25.00	0.10	134.1	-0.011	0.001
2.877	23.16	0.12	1.3	0.000	0.000	2.799	25.16	0.08	134.0	-0.010	0.010
2.886	23.27	0.12	3.3	0.017	0.006	2.824	25.33	0.07	134.6	-0.014	0.011
2.890	23.38	0.09	11.8	0.022	0.008	2.846	25.51	0.06	130.1	-0.011	0.007
2.894	23.50	0.11	8.9	0.023	0.012	2.743	25.72	0.06	127.0	-0.011	0.001
2.898	23.61	0.13	8.4	0.012	0.019	2.772	25.00	0.10	134.1	-0.011	0.001
2.877	23.16	0.12	1.3	0.000	0.000	2.799	25.16	0.08	134.0	-0.010	0.010
2.886	23.27	0.12	3.3	0.017	0.006	2.824	25.33	0.07	134.6	-0.014	0.011
2.890	23.38	0.09	11.8	0.022	0.008	2.846	25.51	0.06	130.1	-0.011	0.007
2.894	23.50	0.11	8.9	0.023	0.012	2.743	25.72	0.06	127.0	-0.011	0.001
2.898	23.61	0.13	8.4	0.012	0.019	2.772	25.00	0.10	134.1	-0.011	0.001
2.877	23.16	0.12	1.3	0.000	0.000	2.799	25.16	0.08	134.0	-0.010	0.010
2.886	23.27	0.12	3.3	0.017	0.006	2.824	25.33	0.07	134.6	-0.014	0.011
2.890	23.38	0.09	11.8	0.022	0.008	2.846	25.51	0.06	130.1	-0.011	0.007
2.894	23.50	0.11	8.9	0.023	0.012	2.743	25.72	0.06	127.0	-0.011	0.001
2.898	23.61	0.13	8.4	0.012	0.019	2.772	25.00	0.10	134.1	-0.011	0.001
2.877	23.16	0.12	1.3	0.000	0.000	2.799	25.16	0.08	134.0	-0.010	0.010
2.886	23.27	0.12	3.3	0.017	0.006	2.824	25.33	0.07	134.6	-0.014	0.011
2.890	23.38	0.09	11.8	0.022	0.008	2.846	25.51	0.06	130.1	-0.011	0.007
2.894	23.50	0.11	8.9	0.023	0.012	2.743	25.72	0.06	127.0	-0.011	0.001
2.898	23.61	0.13	8.4	0.012	0.019	2.772	25.00	0.10	134.1	-0.011	0.001
2.877	23.16	0.12	1.3	0.000	0.000	2.799	25.16	0.08	134.0	-0.010	0.010
2.886	23.27	0.12	3.3	0.017	0.006	2.824	25.33	0.07	134.6	-0.014	0.011
2.890	23.38	0.09	11.8	0.022	0.008	2.846	25.51	0.06	130.1	-0.011	0.007
2.894	23.50	0.11	8.9	0.023	0.012	2.743	25.72	0.06	127.0	-0.011	0.001
2.898	23.61	0.13	8.4	0.012	0.019	2.772	25.00	0.10	134.1	-0.011	0.001
2.877	23.16	0.12	1.3	0.000	0.000	2.799	25.16	0.08	134.0	-0.010	0.010
2.886	23.27	0.12	3.3	0.017	0.006	2.824	25.33	0.07	134.6	-0.014	0.011
2.890	23.38	0.09	11.8	0.022	0.008	2.846	25.51	0.06	130.1	-0.011	0.007
2.894	23.50	0.11	8.9	0.023	0.012	2.743	25.72	0.06	127.0	-0.011	0.001
2.898	23.61	0.13	8.4	0.012	0.019	2.772	25.00	0.10	134.1	-0.011	0.001
2.877	23.16	0.12	1.3	0.000	0.000	2.799	25.16	0.08	134.0	-0.010	0.010
2.886	23.27	0.12	3.3	0.017	0.006	2.824	25.33	0.07	134.6	-0.014	0.011
2.890	23.38	0.09	11.8	0.022	0.008	2.846	25.51	0.06	130.1	-0.011	0.007
2.894	23.50	0.11	8.9	0.023	0.012	2.743	25.72	0.06	127.0	-0.011	0.001
2.898	23.61	0.13	8.4	0.012	0.019	2.772	25.00	0.10	134.1	-0.011	0.001

Table 14. NGC 6851.

$r^{0.25}$	Σ_V	ϵ	θ	a_4	b_4
1.510	19.11	0.25	167.2	-0.002	0.009
1.553	19.31	0.27	166.4	0.007	-0.004
1.506	19.50	0.28	165.8	0.009	0.005
1.641	19.71	0.29	165.1	0.010	-0.001
1.688	19.90	0.30	164.8	0.014	0.009
1.735	20.11	0.29	163.3	0.009	0.005
1.770	20.26	0.30	162.4	0.015	0.011
1.807	20.41	0.29	161.3	0.011	0.006
1.844	20.57	0.28	161.0	0.014	0.004
1.879	20.71	0.28	160.8	0.008	-0.001
1.919	20.87	0.29	160.9	0.007	0.001
1.956	21.02	0.28	160.7	0.000	0.000
1.992	21.17	0.28	160.8	0.004	0.003
2.027	21.32	0.28	161.4	0.006	0.002
2.061	21.48	0.28	160.7	0.004	0.004
2.095	21.63	0.26	162.0	0.007	0.002
2.127	21.79	0.25	162.2	0.010	0.005
2.159	21.94	0.23	162.1	0.011	0.007
2.192	22.10	0.22	163.6	0.012	0.004
2.227	22.25	0.20	164.0	0.015	0.005
2.261	22.41	0.20	166.4	0.010	0.008
2.288	22.51	0.19	165.9	0.014	0.009
2.315	22.62	0.18	166.0	0.011	0.013
2.341	22.73	0.19	166.1	0.014	0.010
2.368	22.83	0.18	166.3	0.014	0.008
2.393	22.94	0.18	169.0	0.017	0.009
2.422	23.05	0.19	171.4	0.015	0.014
2.448	23.16	0.18	172.2	0.016	0.016
2.478	23.27	0.18	174.6	0.011	0.013
2.502	23.38	0.18	174.5	0.014	0.010
2.531	23.51	0.14	165.9	0.000	0.000
2.569	23.61	0.14	138.7	0.000	0.000
2.609	23.73	0.10	105.3	0.000	0.000
2.646	23.85	0.05	114.6	0.000	0.000

Table 15. NGC 6909.

$r^{0.25}$	Σ_V	ϵ	θ	a_4	b_4
1.501	19.51	0.32	71.5	0.011	0.010
1.562	19.71	0.36	69.4	0.014	0.008
1.625	19.91	0.39	68.8	0.009	0.002
1.683	20.11	0.42	69.2	0.007	0.002
1.756	20.31	0.44	68.0	0.002	0.007
1.820	20.51	0.44	69.1	-0.009	0.000
1.864	20.66	0.45	68.8	-0.017	0.001
1.909	20.82	0.44	69.0	-0.008	0.004
1.950	20.97	0.44	68.8	-0.009	0.002
1.989	21.12	0.44	68.7	-0.007	0.001
2.030	21.27	0.45	68.6	-0.007	-0.002
2.068	21.43	0.45	68.7	-0.009	0.002
2.105	21.58	0.45	68.7	-0.011	0.000
2.124	21.73	0.44	69.8	0.000	0.000
2.178	21.89	0.45	68.5	-0.006	0.002
2.216	22.04	0.45	68.5	-0.008	0.002
2.252	22.20	0.46	68.5	-0.012	0.003
2.292	22.35	0.47	68.2	-0.006	0.003
2.331	22.51	0.48	68.2	-0.006	0.003
2.373	22.68	0.50	68.2	-0.011	0.004
2.415	22.83	0.51	67.6	-0.016	0.005
2.446	22.95	0.51	67.6	-0.022	0.002
2.474	23.05	0.51	67.6	-0.023	0.007
2.501	23.16	0.51	67.6	-0.023	0.004
2.530	23.27	0.51	67.5	-0.022	0.001
2.561	23.39	0.52	67.8	-0.014	0.003
2.592	23.50	0.52	67.7	-0.017	0.001
2.625	23.61	0.53	66.9	-0.024	0.008
2.653	23.73	0.53	67.8	-0.018	0.007
2.679	23.85	0.50	69.6	0.000	0.000
2.711	23.97	0.49	72.0	-0.036	0.020
2.754	24.10	0.49	75.4	-0.071	0.021
2.870	24.22	0.54	82.2	-0.100	-0.002
2.918	24.35	0.52	82.8	-0.100	-0.014
2.954	24.49	0.50	82.5	-0.100	-0.030
2.985	24.63	0.48	81.2	-0.100	-0.038

of the 11 galaxies in the sample. Véron-Cetty & Véron (1986) detected nuclear N II emission from this galaxy, but Roberts et al. (1991) failed to find any H I 21-cm emission. Despite the presence of a significant gradient in the Mg_2 index (Carollo et al. 1993), we find no evidence for any significant colour variations.

NGC 4387. Our colour maps do not confirm the presence of the red patch suggested by Ebneter, Djorgovski & Davis (1988).

NGC 4936. This galaxy was included in the Malin & Carter (1980) catalogue of unusual ellipticals as a ‘disturbed system’. The overall light distribution is strongly asymmetric, and our residual map (after subtraction of the averaged model) suggests the presence of shells or ripples (Fig. 14c). Like NGC 2865, this galaxy has a double-peaked H I profile (Boisson et al., in preparation; the gas mass is $\sim 1.1 \times 10^9 M_\odot$). There is also strong nuclear emission from H α , N II, S II and O I. Moreover, there is a bright point-like source ~ 12 arcsec to the SW of the nucleus, which our measurements indicate to be more extended (FWHM ~ 1.4 arcsec) than stars on the same frame (FWHM ~ 0.8 arcsec). This second object may be the nucleus of a merging system. The ($B - I$) colour map (Fig. 15b) and the colour profiles in ($B - V$) and ($V - I$) show that the (main) nucleus is ~ 0.4 mag redder than the surrounding galaxy.

NGC 5831. This system is an excellent match to a simple $r^{0.25}$ profile. A dust lane, ~ 0.05 mag redder than the surrounding galaxy, appears on the ($B - I$) colour map, cutting across the nucleus at a position angle of $\sim 45^\circ$ (Fig. 15c) – see also Ebneter et al. (1988). PDIDC find a weak colour gradient in both ($U - R$) and ($B - R$), but our colour profiles (Fig. 10) are flat.

NGC 5845. This is the smallest galaxy in our sample. Like PDIDC, we find NGC 5845 to be an elliptical with a weak disc and a boxy spheroid, resembling NGC 3610 (Nieto & Bender 1989). There is marginal evidence for a dust lane (or disc-like structure) at most 0.04 mag redder than the adjacent galaxy in the ($B - I$) map.

NGC 6851. Our isophote-fitting indicates that the galaxy is disc-like within the central arcmin (as found by Tonizzone, Stiavelli & Zeilinger 1992), becoming boxy at larger radii. The ($B - I$) colour map shows a well-defined red core, also detected by Véron & Véron-Cetty (1988), and a possible dust lane running approximately north-south across the nucleus (Fig. 15d). Spectra also show that there is weak nuclear N II emission.

NGC 6909. A pure boxy system, this galaxy also has a prominent red nucleus ($\delta(B - I) \sim 0.5$ mag) (Sparks et al. 1985; Véron & Véron-Cetty 1988), while our longer exposures suggest that the reddening extends $\sim 3\text{--}4$ arcsec to the SE of the nucleus itself (Fig. 15e).

4 DISCUSSION

4.1 On colour gradients

One of the main aims of these observations was to search for colour gradients in the outer regions of elliptical galaxies. At least three of the galaxies in our sample (NGC 5831 and 5845, GES, and NGC 3557, Carollo et al. 1993) have been observed spectroscopically and were found to show abundance variations with radius. Neither these galaxies nor any of the other systems in our sample, however, show

statistically significant evidence for monotonic changes in colour with radius. Most have colour profiles that are flat (to within ± 0.03 mag) for surface brightnesses (Σ_V) greater than 25th mag arcsec $^{-1}$ ($r \sim 90$ arcsec in the larger systems), at which radii the random photometric uncertainties become significant (> 0.05 mag – Figs 3–13). Those galaxies that do exhibit colour variations (such as NGC 3258 and 4936) have, like the NGC 6851 observations by Sparks et al. (1991), contradictory ($B - V$) and ($V - I$) gradients, pointing to systematic sky-subtraction problems rather than intrinsic properties.

Accurate sky-subtraction remains the limiting factor for galaxy photometry – a point underlined by the uncertainties in both Σ_V and the ($B - V$), ($V - I$) colours plotted in Figs 3–13. Inaccuracies of as little as 0.5 per cent (2 count pixel $^{-1}$ in V and 0.5 count pixel $^{-1}$ in B for our 30-min, dark-sky frames) have substantial effects at low surface brightness. This point is often emphasized, but not, perhaps, assimilated fully. The average ($B - R$) gradients detected by PDIDC and J87 are only ~ 0.1 mag per decade in radius, while the largest significant extranuclear colour change detected by JFK is 0.05 mag. The gradients measured in ($U - R$) are larger, but we note that, with lower overall quantum efficiency, sky-subtraction is even more problematical in the U band. Echoing JFK, we argue that none of the smaller galaxies studied in previous surveys shows colour gradients larger than the uncertainties, while, even in the larger systems, the gradients and uncertainties are only of the same size.

Is there any evidence for significant colour gradients in ellipticals? We should draw a clear distinction between colour differences in the nuclear ($r < 5$ arcsec) regions of a galaxy and the larger scale gradients discussed above. The central regions of many galaxies have distinctive properties: NGC 6851 and 6909 in our sample have prominent red nuclei; several of the systems studied by de Carvalho, Djorgovski & de Costa (1991) are noticeably redder in the central regions, although none of those objects, nor any of the cluster-centred galaxies studied by Mackie et al. (1990), has significant colour variations outside the central ~ 3 arcsec; finally, many of the galaxies observed by PDIDC and FIH (e.g. NGC 1052, 3377 and 4889) have significantly steeper ($U - R$) gradients in the inner 5–10 arcsec than at larger radii. The characterization of an early-type system by a logarithmic colour gradient, such as $d(B - R)/d \log(r)$, carries the implicit assumption that the abundance varies approximately exponentially with r . If one fits the entire galaxy by a single slope, the (higher signal-to-noise ratio) central colour gradients can have an undue influence on the inferred global properties.

In a similar vein, the broad conclusions drawn from spectroscopic observations can be skewed by substantial nuclear variations. Apart from the observations by GES and by DSP, few galaxies have even Mg_2 measurements that extend more than ~ 10 arcsec from the nucleus. Of the 12 early-type galaxies in the former sample, only NGC 5813 shows a strong trend in Mg_2 beyond the nuclear regions, while five systems (NGC 3818, 3904, 4742, IC 4329, 4296) have nuclear enhancements. Similarly, only five galaxies from DSP (NGC 3379, 4278, 4486, 4636 and, with more scatter, 7626) show smooth Mg_2 gradients extending to large radii, while five others (NGC 351, 741, 3665, 4374 and 4472) have no significant variations in Mg_2 for $R/R_e >$

0.2. Thus, while metallicity variations clearly are present in these systems, a core-halo structure is at least as plausible as a continuous gradient for more than half of the sample.

In summary, our results show no evidence for significant, large-scale BVI colour gradients in the ellipticals in our sample. Moreover, we argue that, by accurately taking account of the systematic uncertainties involved in sky subtraction at low light levels, we weaken much of the evidence for large-scale effects that has been presented in previous studies, although these overall colour gradients should be distinguished from nuclear colour variations. Three galaxies in our sample have spectroscopically measured abundance variations. Our failure to find any corresponding photometric variations suggests that the latter may be significantly more subtle than previously believed.

4.2 Structure

In our small sample of 11 galaxies, three systems – NGC 3258, 3268 and 3557 – show minor or no significant deviations from pure ellipticity. Of the others, NGC 4387 and 6909 are pure boxy systems with low systemic rotational velocities. The remaining systems (NGC 2865, 3091, 4936, 5845 and 6851) all have a_4 coefficients indicative of pointed isophotes at some radii. All, however, also have significant (2–4 per cent) $\sin(4\theta)$ terms in the Fourier decomposition, and, with the available data, it is not possible to distinguish between the presence of a weak disc and projection effects in triaxial systems (FIH), although three galaxies, NGC 4936, 5845 and 6851, also show significant isophote twists, favouring the latter interpretation. Indeed, even in the case of NGC 5831, which appears to have a faint inner disc, projection effects may explain the abrupt change in position angle and ellipticity. A full study of these questions requires extensive modelling of triaxial systems, which is beyond the scope of the present investigation.

Dust is present in several systems; it is marginally detected in NGC 5831 and 5845, and clearly present in NGC 6851 and 6909. These galaxies span the full range of morphological parameters – discy to boxy, low luminosity to high luminosity. Finally, NGC 4936 and 3091 are shell galaxies. Together with NGC 2865 (Fort et al. 1986) and NGC 6776 (SRB), this means that four of the 12 galaxies in our sample (and four of the nine high-luminosity systems) have features that are probably due to relatively recent mergers. Although our sample is small, this fraction is consistent with the results of the Schweizer & Seitzer (1992) survey.

5 CONCLUSIONS

We have presented BVI photometry of a sample of 11 early-type galaxies, which extends to objects at least twice as faint as in previous studies. We have taken particular care in determining the sky-background level in these observations, obtaining adjacent, overlapping CCD frames for the more luminous galaxies. None of the systems, spanning a wide range in luminosity and morphological characteristics, shows evidence for significant colour gradients at distances beyond ~ 5 arcsec from the nucleus. Indeed, most of the systems have ($V - I$) colours that are constant to within ± 0.03 mag to radii of 50 arcsec or more. From our observations, it is clear that an accurate measurement of colours at these radii

demands extremely accurate sky-subtraction; systematic errors of as little as 0.5 per cent introduced apparent gradients comparable with those found in previous surface photometry analyses. [Nuclear ($r \lesssim 10$ arcsec) gradients are more common.] Based on our observations and a re-examination of those in the literature, we argue that few elliptical galaxies have significant large-scale colour gradients, and that the broad-band photometric properties may not be good tracers of the metal abundance in these systems.

ACKNOWLEDGMENTS

INR thanks the Observatoire de Paris, Meudon for hospitality on several occasions over the last five years. We also thank P. Prugniel for initial help with the PLEINPOT package, and U. Jorgenson for making available the JFK data in digital form. This work was based on observations obtained at the European Southern Observatory, La Silla, Chile.

REFERENCES

- Bender R., Döbereiner S., Möllenhoff C., 1987, *A&AS*, 74, 385
 Bender R., Surma P., Döbereiner S., Möllenhoff C., Madejsky R., 1989, *A&A*, 217, 35
 Bertola F., Cappacioli M., 1975, *ApJ*, 200, 439
 Binney J., 1978, *MNRAS*, 183, 501
 Binney J., 1982, *MNRAS*, 200, 951
 Birkinshaw M., Davies R. L., 1985, *ApJ*, 291, 32
 Boroson T. A., Thompson I. B., 1991, *AJ*, 101, 111
 Burstein D., Davies R. L., Dressler A., Faber S. M., Stone R. P. S., Lynden-Bell D., Terlevich R. J., Wegner G., 1987, *ApJS*, 64, 601
 Carollo C. M., Danziger I. J., Buson L., 1993, *MNRAS*, 265, 553
 Carter D., 1987, *ApJ*, 312, 514
 Davidge J. T., 1992, *AJ*, 103, 1512
 Davies R., Efstathiou G., Fall M., Illingworth G., Schechter P., 1983, *ApJ*, 266, 41
 Davies R. L., Sadler E. M., Peletier R. F., 1993, *MNRAS*, 262, 650 (DSP)
 de Carvalho R. R., Djorgovski S., da Costa L. N., 1991, *ApJS*, 76, 1067
 Delisle S., Hardy E., 1992, *AJ*, 103, 711
 de Vaucouleurs G., 1948, *Ann. Astrophys.*, 11, 247
 de Vaucouleurs G., 1953, *MNRAS*, 113, 134
 Djorgovski S., 1985, PhD thesis, Univ. California, Berkeley
 Dupraz C., Combes F., 1987, *A&A*, 185, L1
 Ebnetter K., Djorgovski S., Davis M., 1988, *AJ*, 98, 538
 Eggen O., Sandage A., 1964, *ApJ*, 140, 130
 Faber S. M., Wegner G., Burstein D., Davies R. L., Dressler A., Lynden-Bell D., Terlevich R. J., 1989, *ApJS*, 69, 763
 Fort B. P., Prieur J.-L., Carter D., Meatheringham S. J., Vigroux L., 1986, *ApJ*, 306, 110
 Franx M., Illingworth G. D., Heckman T., 1989, *ApJ*, 344, 613 (FIH)
 Gorgas J., Efstathiou G., Aragon-Salamanca A., 1990, *MNRAS*, 245, 217 (GES)
 Jedrzejewski R., 1987, *MNRAS*, 226, 747 (J87)
 Jorgenson U. G., Franx M., Kjaergaard P., 1992, *A&AS*, 95, 489 (JFK)
 Kent S., 1984, *ApJS*, 56, 105
 Kormendy J., Sanders D., 1992, *ApJ*, 390, L53
 Lauer T., 1985, *ApJS*, 57, 473
 Mackie G., Visvanathan N., Carter D., 1990, *ApJS*, 73, 637
 McNamara B. R., O'Connell R. W., 1992, *ApJ*, 393, 579
 Malin D., Carter D., 1980, *Nat*, 285, 643
 Malin D., Carter D., 1983, *ApJ*, 274, 534
 Nieto J., Bender R., 1989, *A&A*, 215, 266
 Peletier R. F., 1989, PhD thesis, Univ. Groningen
 Peletier R. F., Davies R. L., Illingworth G. D., Davis L. E., Cawson M., 1990, *AJ*, 100, 1091 (PDIDC)
 Quinn P., 1984, *ApJ*, 279, 256
 Roberts M. S., Hogg D. E., Bregman J. N., Forman W. R., Jones C., 1991, *ApJS*, 75, 751
 Sansom A. E., Reid I. N., Boisson C., 1988, *MNRAS*, 234, 247
 Schild R. E., 1983, *PASP*, 95, 1021
 Schweizer F., 1982, *ApJ*, 252, 455
 Schweizer F., Seitzer P., 1992, *AJ*, 104, 1039
 Sparks W. B., Wall J. V., Thorne D. J., Jorden P. R., van Breda I., Rudd P., Jorgenson H., 1985, *MNRAS*, 217, 87
 Sparks W. B., Wall J. V., Jorden P. R., Thorne D. J., van Breda I., 1991, *ApJS*, 76, 471
 Stavelli M., Prugniel P., Zeilinger W. W., 1991, in Grosbol P. J., Warmels R. H., eds, 3rd ESO/ST-ECF Data Analysis Workshop, ESO, Garching, p. 231
 Stobie R. S., Sagar R., Gilmore G. F., 1987, *A&AS*, 60, 503
 Tonazzio T., Stavelli M., Zeilinger W. W., 1992, *A&A*, 259, 39
 Toomre A., Toomre J., 1972, *ApJ*, 178, 623
 Vader J., Vigroux L., Lachiéze-Rey M., Souviron J., 1988, *A&A*, 203, 17
 Véron P., Véron-Cetty M. P., 1988, *A&A*, 204, 28
 Véron-Cetty M. P., Véron P., 1986, *A&AS*, 66, 335
 Vigroux L., Souviron J., Lachiéze-Rey M., Vader J., 1988, *A&AS*, 73, 1
 Wright G. S., James P. A., Joseph R. D., McLean I. S., 1990, *Nat*, 344, 417